DISSERTATION

submitted to the

Combined Faculty of Natural Sciences and Mathematics

of the Ruprecht-Karls-University of Heidelberg, Germany

for the degree of

Doctor of Natural Sciences

Presented by

Johannes Gahn

Master of Science

Born in: Erlangen, Germany

Oral examination: 12th May 2025

The role of Smad signaling in maintaining hemodynamic homeostasis

Referees: Prof. Dr. Thomas Wieland

Jun.-Prof. Dr. Roxana Ola

Corrigendum

As per my PhD defense committee members, it was decided that my initial submitted version of the thesis does not delineate clearly the authorship of each individual experiment.

The discrepancies between the previous version and the present one, are outlined as follows. The term "Old" denotes the inaccurate version, while "New" signifies the accurate version. Page numbers pertain to the written pages rather than the PDF pagination.

1) Page 14:

Old: To validate the RNA sequencing findings, I performed quantitative real-time polymerase chain reaction (RT-PCR) on SMAD4 siRNA HUVECs in comparison with CTRL siRNA subject to a gradient of shear stress (1-5-12 DYNES/cm²) for 2 hours.

New:

To validate the RNA sequencing findings, **Ms. Kuheli Banerjee** performed quantitative real-time polymerase chain reaction (RT-PCR) on SMAD4 siRNA HUVECs in comparison with CTRL siRNA subject to a gradient of shear stress (1-5-12 DYNES/cm²) for 2 hours.

2) Page 14: Legend for Figure 8:

Old:

SMAD4 (B) and KLF4 (C) mRNA expression after exposure to 1, 5, and 12 dynes for 24 hours (n=5). Data is shown as mean ± SEM.

New:

SMAD4 (B) and KLF4 (C) mRNA expression after exposure to 1, 5, and 12 dynes for 24 hours (n=5). **(B and C) performed by Ms. Kuheli Banerjee.** Data is shown as mean ± SEM.

3) Page 15:

Old:

To validate the restrictive role of SMAD4 in FSS-induced Klf4 activation in vivo, dissected retinas from postnatal day 6 (P6) tamoxifen-induced *Smad4* fl/fl and *Smad4*$^{i\Delta EC}$ mice were immunolabelled for KLF4 and Isolectin B4 (IB4) to visualize the vasculature.

New:

To validate the restrictive role of SMAD4 in FSS-induced Klf4 activation in vivo, dissected retinas from postnatal day 6 (P6) tamoxifen-induced *Smad4* fl/fl and *Smad4*$^{i\Delta EC}$ mice were immunolabelled, **by Ms. Kuheli Banerjee** for KLF4 and Isolectin B4 (IB4) to visualize the vasculature.

4) Page 15: Legend for Figure 9:

Old:

The ratio of Klf4 positive cells per vessel length is shown in (E), and the respective pixel intensity in (F) (n=6). Experiments performed by Ms. Kuheli Banerjee. Data represented as mean ± SEM.

New:
The ratio of Klf4 positive cells per vessel length is shown in (E), and the respective pixel intensity in (F) (n=6). **(A-F)** Experiments performed by Ms. Kuheli Banerjee. Data represented as mean ± SEM.

5) Page16:
Old:
To further investigate the role of Klf4 in the pathogenesis of AVMs, we (myself and Kuheli Banerjee) employed an in vivo model to assess AVM formation.
New:
To further investigate the role of Klf4 in the pathogenesis of AVMs, **Ms. Kuheli Banerjee** employed an in vivo model to assess AVM formation.

6) Page 16: Legend for Figure 10:
Old:
Quantification of the AVM number (C). Experiments conducted by Ms Kuheli Banerjee. Data is shown as mean ± SEM.

New:
Quantification of the AVM number (C). **(A-D)** Experiments conducted by Ms. Kuheli Banerjee. Data is shown as mean ± SEM.

7) Page17:
Old:
To assess whether KLF4 operates upstream of PI3K signaling, I measured pAkt in static versus 2 hours of P-FSS conditions upon depletion of KLF4 or SMAD4 alone or in combination KLF4;SMAD4 by Western blot.

New:
To assess whether KLF4 operates upstream of PI3K signaling, **Ms. Kuheli Banerjee** measured pAkt in static versus 2 hours of P-FSS conditions upon depletion of KLF4 or SMAD4 alone or in combination KLF4;SMAD4 by Western blot.

8) Page 17: Legend for Figure 11:
Old:
Western blot for pAkt, Akt, PECAM, and GAPDH in CTRL, SMAD4, KLF4, or SMAD4;KLF4 transfected HUVECS subjected to 12DYNEs/cm2 for 2 hours (B). Experiments performed by Ms. Kuheli Banerjee. Quantification of pAkt (n=6) levels (C).

New:
Western blot for pAkt, Akt, PECAM, and GAPDH in CTRL, SMAD4, KLF4, or SMAD4;KLF4 transfected HUVECS subjected to 12DYNEs/cm2 for 2 hours (B). **(A-C)** Experiments performed by Ms. Kuheli Banerjee. Quantification of pAkt (n=6) levels (C).

9) Page 18:
Old:
To validate these results and further investigate the FSS-dependent regulation of these genes upon KLF4, I conducted RT-PCR on HUVECs with KLF4 depletion in both static and 2-hour P-FSS conditions.
New:
To validate these results and further investigate the FSS-dependent regulation of these genes upon KLF4, **Ms. Kuheli Banerjee** conducted RT-PCR on HUVECs with KLF4 depletion in both static and 2-hour P-FSS conditions.

10) Page 18:
Old:
To elucidate whether KLF4 directly regulates TEK, I further assessed TEK expression in cells overexpressing KLF4 (KLF4OE) using RT-PCR analysis.
New:
To elucidate whether *KLF4* directly regulates *TEK*, **Ms. Yanzhu Lin** further assessed *TEK* expression in cells overexpressing *KLF4 (KLF4OE)* using RT-PCR analysis.

11) Page 18: Legend for Figure 12:
Old:
RT-PCR analysis of TEK in CTRL and KLF4OE cells (n=4). Data is shown as mean ± SEM.
New:
RT-PCR analysis of TEK in CTRL and KLF4OE cells (n=4). **Experiments in (B) conducted by Ms. Kuheli Banerjee and in (C) by Ms. Yanzhu Lin**. Data is shown as mean ± SEM.

12) Page 18:
Old:
To validate the requirement of TEK in KLF4-mediated Akt signaling, TEK was deleted in CTRL versus KLF4OE HUVECs subject to FSS for 2 hours.
New:
To validate the requirement of TEK in KLF4-mediated Akt signaling, **Ms. Kuheli Banerjee** deleted TEK in CTRL versus KLF4OE HUVECs subject to FSS for 2 hours.

13) Page 19: Legend for Figure 13:
Old:
Quantification of pAkt (C) and TEK(D) protein levels. Ms. Kuheli Banerjee performed WB experiments. Data represented as mean ±SEM.
New:
Quantification of pAkt (C) and TEK (D) protein levels. Ms. Kuheli Banerjee performed WB experiments **(B-D)**. Data represented as mean ±SEM.

Johannes Gahn
04.06.2025

Acknowledgments

I am writing to express my sincere appreciation to everyone who has supported and contributed to completing my doctoral thesis along the way.

To begin with, I want to extend my heartfelt thanks to my thesis supervisor, Jun. Prof. Roxana Ola, for her support and for believing in me with this ambitious undertaking. I am grateful for your assistance throughout the ups and downs of the past five years. You have been an exceptional mentor. You have always addressed my questions from day one, helped me plan and execute experiments, and interpreted the findings.

I feel fortunate to have had a highly encouraging and supportive thesis committee. I am grateful to Prof. Thomas Wieland and Prof. Dr. Adelheid Cerwenka for their guidance, fresh ideas, motivation, shared reagents, and expertise that helped me complete my project. I feel incredibly honored and privileged to be part of the Heidelberg Biosciences International Graduate School (HBIGS). I want to acknowledge the entire HBIGS team and student community for their tremendous support, from facilitating my registration at the faculty to organizing career and academic courses that have shaped me as a researcher.

I sincerely appreciate Prof. Gergana Dobreva and her research group for consistently providing me with reagents and critical scientific insights-special thanks to Dr. rer. nat. Julio Cordero, thank you for all the bioinformatics training and advice you gave regarding analyzing my datasets.

The achievements of my thesis project and other endeavors are a testament to the invaluable support of my skilled lab mates, Kuheli Banerjee and Yanzhu Lin. Since our group's formation, we have worked closely together, progressing in tandem to get to this point. Kuheli, thank you for all your time with me in the animal house. It has been a joy to collaborate with you. Lin, I am incredibly thankful for your patience as I learned to dissect retinas. Your encouragement, lively discussions, innovative ideas, and constructive feedback have been essential. Your presence has dramatically enhanced the atmosphere in our lab, and I am truly grateful for everything. I would also like to thank my other lab mates, Tanmaya, Yuxi, and Zohra, for consistently maintaining a positive lab spirit and all their assistance.

My research would not have progressed without the support of all the lab technicians: Tina, Sabine, Doris, and Heinz. I appreciate all the assistance in the lab. I would also like to express my gratitude to the members of AG Wieland, Santhosh, Yohannes, and Nabil for their delightful conversations and all their support.

My life would have been quite different without my friends. I am very grateful for all your motivation. Thank you for always being there for me and making my life enjoyable.

Finally, I am grateful to my family for their unwavering support, understanding, and encouragement throughout this journey. Their love, belief in me, and patience have motivated me constantly.

Table of Contents

List of Figures

List of Tables

Summary

In the present study, I have investigated the cellular molecular and mechanisms regulated by the crosstalk between fluid shear stress (FSS) and canonical BMP9/10 signaling pathway, whose dysregulation leads to the formation of arteriovenous malformations (AVMs), a pathogenic feature of dysfunctional SMAD4 signaling in endothelial cells (ECs).

Interestingly, in the first part of my study, I found that BMP9/10 signaling pathway through SMAD4 acts upstream of FSS to restrict FSS-mediated *KLF4* induction that tempers the downstream Akt activation. And this mechanism is required to maintain EC quiescence and vascular homeostasis. Thus, upon loss of Smad4 in the ECs two pools of PI3K/Akt hyperactivation occur: one through transcriptional de-repression of casein kinase (CK2) and resultant inactivation of PTEN and the second one that is specific to the high-flow AVMs through upregulation of KLF4 driving an increase in the receptor tyrosine kinase, TIE2 expression that further exacerbates PI3K/Akt signaling activation. These findings highlight the role of RTKs other than the well-known VEGFRs in regulating EC mechano-transduction signaling events.

In the second part of my study I was interested in identifying the KLF4-TIE2-Akt upstream regulatory mechanisms governed by SMAD4 signaling. Interestingly, I identified another RTK, KIT, that independently of its ligand stem cell factor (SCF) acts upstream of KLF4 and Akt activation. I identified that KIT is regulated by the BMP9/10-FSS crosstalk and furthermore SMAD4 signaling is required for FSS mediated KIT downregulation irrespective of FSS magnitude. Thus, is Smad4 LOF ECs, KIT expression is upregulated and mediated excessive ERK5 activation, an upstream event that regulates KLF4 induction upon FSS. Increased Kit-Erk5 pathway was further validated in vivo in neonatal retinas with EC specific *Smad4* depletion. KIT was found also within the AVMs in HHT patient biopsies. Lastly, the inhibition of Kit using a selective inhibitor was able to rescue AVM formation in mouse retinas, providing evidence that targeting RTKs can potentially mitigate AVM development. These findings outline a complex signaling network involving SMAD4, PI3K/AKT, KIT, ERK5, and KLF4, revealing RTKs as key modulators of endothelial responses to FSS and AVM pathology. These results suggest that RTKs, particularly KIT and TIE2, play a crucial role in the pathogenesis of AVMs and highlight their potential as therapeutic targets for treating AVM-related vascular abnormalities.

Zusammenfassung

In der vorliegenden Studie habe ich die molekularen und zellulären Mechanismen untersucht, die durch das Zusammenspiel zwischen Flüssigkeitsstress (FSS) und dem kanonischen BMP9/10-Signalweg reguliert werden. Diese Dysregulation führt zur Bildung arteriovenöser Malformationen (AVMs), einem pathogenen Merkmal einer dysfunktionalen SMAD4-Signalübertragung in Endothelzellen (ECs).

Interessanterweise habe ich im ersten Teil meiner Studie herausgefunden, dass der BMP9/10-Signalweg über SMAD4 vorgeschaltet auf die FSS induzierte Signalkaskade wirkt, um die FSS-vermittelte KLF4-Induktion einzuschränken, die nachgeschaltete Akt-Aktivierung abschwächt. Dieser Mechanismus ist für die Aufrechterhaltung der Ruhephase von EC und der vaskulären Homöostase erforderlich. Nach dem Verlust von Smad4 in ECs kommt es also zu zwei verschiedenen Arten der PI3K/Akt-Hyperaktivierung: zum einen durch die transkriptionelle Depression der Kaseinkinase (CK2) und die daraus resultierende Inaktivierung von PTEN und zum anderen, spezifisch für die AVMs mit hohem FSS, durch die Hochregulierung von KLF4, die zu einem Anstieg der Expression der Rezeptortyrosinkinase TIE2 führt, was die Aktivierung der PI3K/Akt-Signale weiter verstärkt. Diese Ergebnisse unterstreichen die Rolle anderer RTKs als der bekannten VEGFRs bei der Regulierung der FSS-Signalereignisse in den Zellen.

Im zweiten Teil meiner Studie war ich daran interessiert, die vorgelagerten KLF4-TIE2-Akt-Regulationsmechanismen zu identifizieren, die von der SMAD4-Signalgebung gesteuert werden. Interessanterweise habe ich eine weitere RTK, KIT, identifiziert, der unabhängig von seinem Liganden Stammzellfaktor (SCF) KLF4 reguliert. Ich habe herausgefunden, dass KIT sowohl durch BMP9/10 als auch durch FSS geregelt wird und darüber hinaus, dass die SMAD4-Signalkaskade für die FSS-vermittelte KIT Herunterregulierung erforderlich ist. In ECs mit SMAD4- Funktionsverlust wird die KIT-Expression also hochreguliert und durch eine exzessive ERK5-Aktivierung vermittelt diese die KLF4-Induktion bei FSS. Der verstärkte Kit-Erk5-Signalweg wurde in vivo in neonatalen Netzhäuten mit EC-spezifischer Smad4-Depletion weiter validiert. KIT wurde auch in den AVMs in Biopsien von HHT-Patienten gefunden. Schließlich konnte die Hemmung von KIT mit einem selektiven Inhibitor die AVM-Bildung in Mäusen retten, was beweist, dass eine gezielte Beeinflussung von RTKs die AVM-Entwicklung möglicherweise abschwächen kann. Diese Ergebnisse skizzieren ein komplexes Signalnetzwerk, an dem SMAD4, PI3K/AKT, KIT, ERK5 und KLF4 beteiligt sind, und zeigen, dass RTKs Schlüsselmodulatoren der endothelialen Reaktionen auf FSS und AVM-Pathologie sind. Diese Ergebnisse deuten darauf hin, dass RTKs, insbesondere KIT und TIE2, eine entscheidende Rolle bei der Pathogenese von AVMs spielen und weisen auf ihr Potenzial als therapeutische Ziele für die Behandlung von AVM-bedingten Gefäßanomalien hin.

1. Introduction

1.1 Hereditary Hemorrhagic Telangiectasia (HHT)

Hereditary Hemorrhagic Telangiectasia (HHT) is a rare autosomal dominant genetic condition, with an estimated prevalence of approximately 1 in 5.000 individuals, commonly referred to as Osler-Weber-Rendu syndrome. Clinically, HHT is a vascular disorder characterized by torturous direct connections between feeding arteries and draining veins, with no intervening capillary bed. HHT manifests through either small, dilated blood vessels known as telangiectasias (Figure 1A, B) that appear as mucocutaneous lesions located in the skin, buccal mucosa, and nasal cavity, and/or larger caliber arteriovenous malformations (AVMs) encountered, particularly within visceral organs (Figure 1 C-F) [1-4].

These abnormal hypoxic connections exhibit impaired nutrient exchange and inadequate regulation of capillary dynamics. In contrast to high-resistance capillary networks, AVMs cannot modulate blood flow, which can result in structural remodeling and dilatation of the draining veins. Such pathological alterations can culminate in tissue necrosis, morphological abnormalities, ischemic conditions, cerebrovascular accidents, and, in extreme instances, congestive heart failure [5]. Telangiectasias are commonly observed in the nasal mucosa, whilst AVMs occur within vital organs, including the brain, lungs, liver, and gastrointestinal tract (GI). The increased blood flow associated with these lesions renders them fragile and susceptible to rupture. This can lead to recurrent episodes of epistaxis, contributing to anemia or internal hemorrhage in the case of AVMs, both of which pose severe, potentially life-threatening conditions [6].

Treatment for HHT typically focuses on managing the symptoms and preventing their complications. This may involve using medications such as antifibrinolytics to reduce the bleeding and iron supplements to address anemia. In more severe cases, surgical interventions, such as embolization of AVMs or laser therapy to treat vascular lesions, may be necessary. Ongoing monitoring for complications, particularly pulmonary and brain AVMs, is crucial. Recent research has also explored targeted therapies, including monoclonal antibodies like bevacizumab, to reduce abnormal vessel growth [6-8].

HHT is primarily attributed to heterozygous loss-of-function (LOF) mutations in genes involved in the Bone morphogenic proteins (BMP) 9 and 10 signaling pathway [9]. Haploinsufficiency alone does not account for the focal formation of AVM lesions in the context of a systemic mutation, leading to a two-hit hypothesis, where the second hit may involve a somatic mutation or an angiogenic or environmental factor, such as tissue injury, mechanical stress, or radiation exposure, that triggers the lesions [10, 11]. Approximately 90% of HHT cases are attributed to heterozygous mutations in the activin receptor-like kinase 1 (*ACVRL1* or *ALK1*) gene, causing type 2 HHT (HHT2), or in the *ENG* gene encoding Endoglin, responsible

for type 1 HHT (HHT1) [12, 13]. Less commonly (1-2%), mutations in the downstream SMAD family member 4 (*SMAD4*) gene, encoding for the transcriptional effector SMAD4, cause juvenile polyposis HHT (JP-HHT) [14]. Furthermore, a rare subset of patients (less than 1%) exhibiting an HHT-like phenotype are identified with mutations in the growth and differentiation factors 2 (*GDF2*) gene, which encodes for the growth factor BMP9 [15].

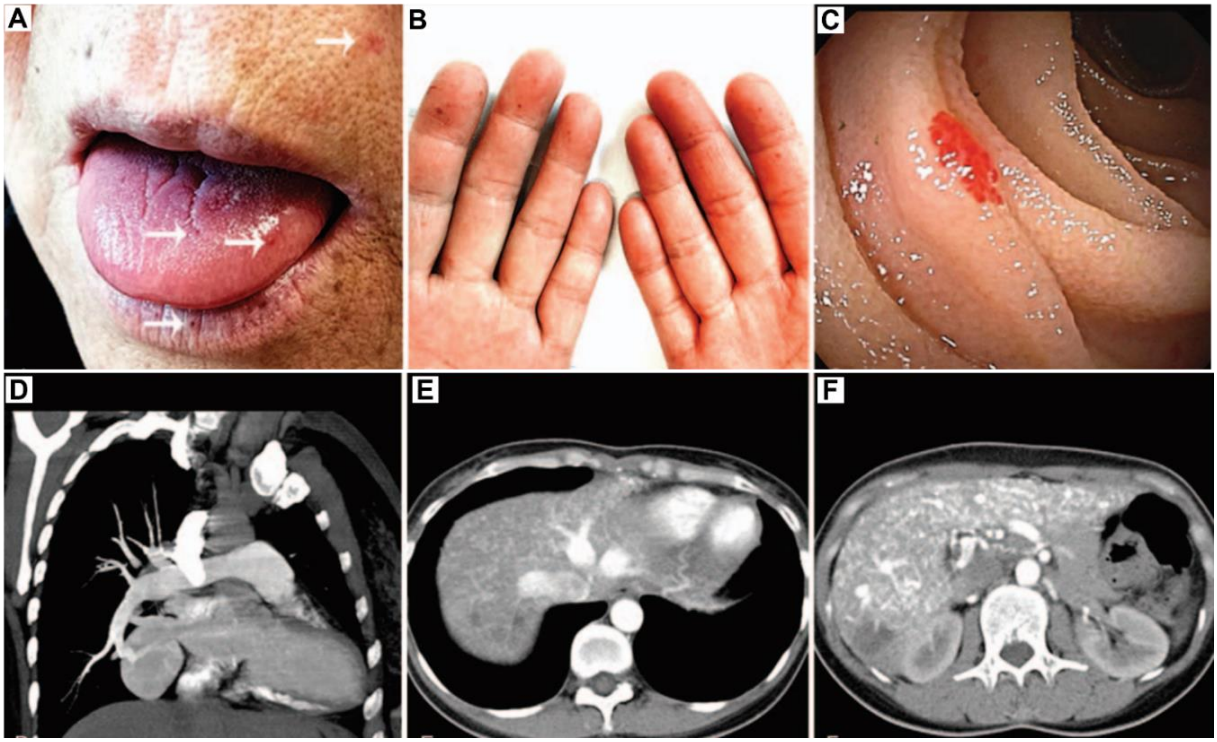

Figure 1: **HHT clinical appearance**: small telangiectasias were in the mucosal tissues of the lips, tongue, and fingers (A and B). Enteroscopy images of telangiectasias throughout the GI tract (C). Contrast-enhanced computed tomography (CT) scans of a 35-year-old woman with HHT show hepatic AVMs (D), hepatic arteriovenous shunts (E), and in (F), arterioportal shunts. Image adapted from [16].

1.2 Bone morphogenic protein 9/10 signaling pathway

The BMP signaling pathway is a crucial regulatory mechanism that regulates fundamental biological processes in mammals, including cell differentiation, growth, apoptosis, migration, and tissue patterning [17]. BMPs are part of the transforming growth factor-beta (TGF-β) superfamily and were initially identified for their capacity to induce osteogenesis [18]. However, it has since been established that BMPs regulate a broad spectrum of cellular functions encompassing cell differentiation, proliferation, apoptosis, and migration [19].

BMP ligands have been categorized into subgroups based on their sequence similarity, receptor affinities, and functional characteristics. These include the BMP-2 and BMP-4 subgroup, the BMP-5, BMP-6, BMP-7, and BMP-8 subgroup, the BMP-9 and BMP-10 subgroup, and the GDF5, GDF6, and GDF7 subgroup [20].

1.2.1 Structure and Activation of BMP Signaling

BMP signaling commences upon BMP ligand binding to a heterotetrameric receptor complex on the surface of target cells. This receptor complex comprises type I and type II serine/threonine kinase receptors. Upon ligand binding, the type II receptors, such as BMP receptor type II (BMPRII), activin receptors II A and II B (ActRII, or ActRIIB), phosphorylate and activate type I receptors, including BMP receptors type I A or B (BMPRIA, BMPRIB), or ALK1 [21]. Some receptor complexes may also include type III receptors, such as Endoglin or Betaglycan, or co-receptors that further modulate the ligand-receptor binding affinities [22]. Upon activation, the type I receptor transmits the signal intracellularly by phosphorylating specific downstream effectors referred to as receptor-regulated SMADs (R-SMADs: SMAD1/5/8). Subsequently, the phosphorylated R-SMADs bind to the common mediator SMAD (Co-SMAD), identified as SMAD4, to form a complex that translocates from the cytoplasm to the nucleus. Within the nucleus, this complex orchestrates the transcriptional regulation of target genes [23].

1.2.2 Role of BMP9 and BMP10 in Endothelial Cell Function

BMP9 and BMP10 are closely related members of the BMP family with similar functions. BMP9 is generated in hepatic stellate cells in the liver [24], while BMP10 is mainly produced by cardiomyocytes [25].

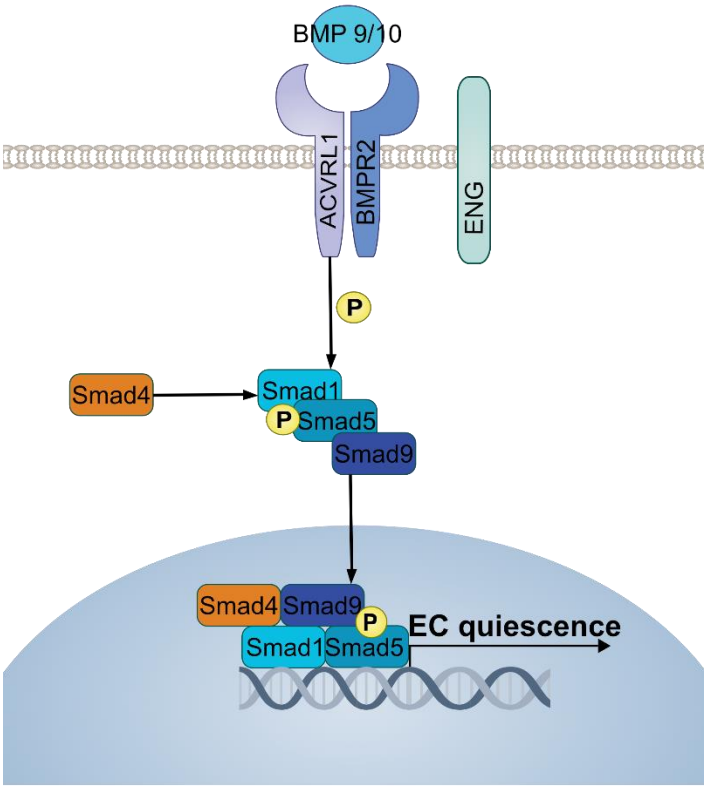

Figure 2: **BMP9 and 10 signaling pathway:** BMP9 and 10 engage with the heterotetrameric BMP receptor complex, activating the canonical SMAD signaling pathway, specifically SMAD1, 5, and 9. The R-SMADs subsequently form complexes with SMAD4, and the SMAD complexes translocate from the cytoplasm to the nucleus, where they exert regulatory control over gene transcription.

Both ligands are secreted into the bloodstream and exhibit high-affinity binding to the receptor ALK1 on the endothelial cell (EC) surface, thereby activating the canonical SMAD1/5/9 – SMAD4 signaling pathway [26] (Figure 2). The levels of the ligands in the plasma are high during embryogenesis and soon after birth when developmental angiogenesis remains active and decreases with age when vascular quiescence is achieved and vascular homeostasis is established.

BMP9 and BMP10 enhance EC stability and maintain vascular homeostasis by inhibiting excessive proliferation and migration [27]. BMP9/10 govern vascular quiescence by opposing the activation of vascular endothelial growth factor receptor 2 (VEGFR2) upon its ligand, vascular endothelial growth factor A (VEGFA) stimulation and subsequently block the activation of downstream signaling pathways such as Akt and extracellular signal-regulated kinase (ERK) [28]. Furthermore, BMP9 curtails the activation of phosphoinositide 3-kinase (PI3K) signaling in ECs by inhibiting the phosphorylation of phosphatase and tensin homolog (PTEN) via the direct transcriptional repression of casein kinase 2 (CK2) [29]. Upon phosphorylation, PTEN engages in closed conformation, being unable to bind the cell membrane and inactivate PI3K, resulting in an increased Akt activation. These modulations are essential for averting uncontrolled vascular expansion or remodeling, leading to pathological conditions, including vascular malformations.

1.3 Murine models of HHT

HHT murine models predominantly investigate the inactivation of genes associated with the BMP9/10 signaling pathway, notably *Eng*, *Acvrl1,* and *Smad4*. These models replicate significant characteristics of HHT pathology, encompassing AVMs, telangiectasia, and an increased vulnerability to hemorrhagic events. Their application has played a critical role in clarifying the molecular mechanisms that contribute to vascular anomalies and has provided vital insights into potential therapeutic strategies for treating HHT.

Global deletion of *Eng* or *Acvrl1* in mice results in significant defects in yolk sac angiogenesis, as evidenced by delayed maturation of embryonic vascular structures and diminished coverage of vascular smooth muscle cells (vSMCs). These alterations ultimately lead to early embryonic lethality. Notably, vasculogenesis appears to proceed normally in these cases, indicating that *Eng* and *Acvrl1* are essential for angiogenesis rather than the initial development of the primitive vascular plexus [30-33].

Global heterozygous knockout mice (*Eng*+/- and *Acvrl1*+/-) exhibit a genotype that closely mirrors that of patients with HHT. Both murine models develop vascular lesions reminiscent of HHT-like pathologies between the ages of 7 and 20 months. These lesions include capillary dilation across various organs and instances of hemorrhage [34]. Notably, the manifestation of these lesions is characterized by incomplete penetrance and unpredictability. In contrast to

human patients, these mice do not exhibit spontaneous AVM formation. However, brain AVMs (bAVMs) arise in response to external stimuli, such as VEGFA [35].

Recent developments in the field utilizing mouse models with the inducible Cre/Lox system to ablate the ligands *Gdf2* and/or *Bmp10* [36], the receptors: *Eng* [37] *Acvrl1* [38], the Smad factors *Smad1/5* [39] or *Smad4* [29, 40] have shown that the EC-specific deletion of either of these genes results in AVM formation, suggesting that impaired function of BMP9/10 signaling in the ECs is the source of AVMs. Yet, AVM development in these murine models of HHT requires the deletion of both alleles and active angiogenesis, indicating additional contributors to AVM development in the HHT patients. These findings emphasize the exclusive role of canonical BMP9/10 signaling in vascular homeostasis in protecting the endothelium against AVM formation.

1.3.1 Eng Knockout Mouse Model

EC-specific deletion of *Eng* in neonates leads to the formation of AVMs in the retinas, brain, and lung, as well as in the pelvic region. The later AVMs lead to increased workload and cardiac hypertrophy. In adult mutant mice, skin AVMs are induced upon wounding-mediated inflammation [41-43] (Figure 3).

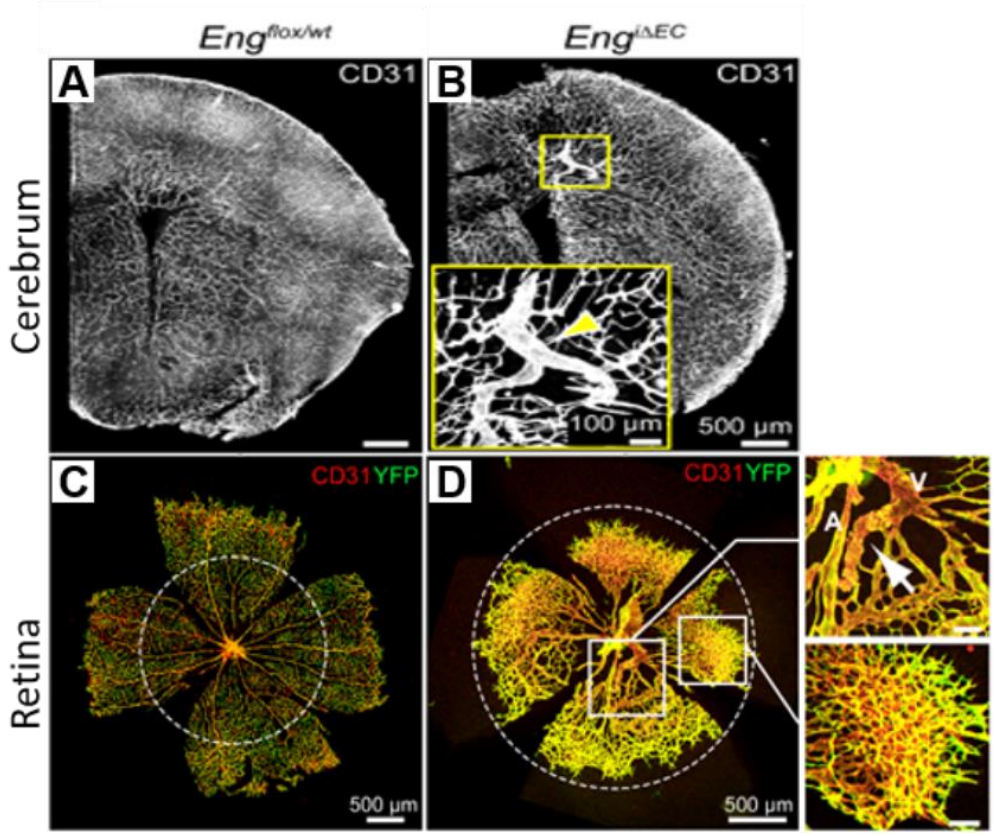

Figure 3: **EC-specific *Eng* loss of function causes local AVMs:** The vascular architecture of developing brains from control mice (A) and tamoxifen-induced *Eng* depletion (B). The boxed region highlights an AVM. Retinal vasculature from control (C) and EC-specific *Eng* deletion (D), AVM, and the sprouting retinal front delineated by boxed region. A: artery; V: vein. Adapted from [44].

1.3.2 *Acvrl1* Knockout Mouse Model

Much like the EC-specific deletion of *Eng, Alk1* deletion in neonatal ECs results in cerebral and pulmonary as well as retinal AVMs [45]. However, the deletion of *Alk1* results in the development of anemia, GI hemorrhages, and AVMs in adult mice, while the analogous deletion of *Eng* does not phenocopy GI tract anomalies [46, 47] (Figure 4).

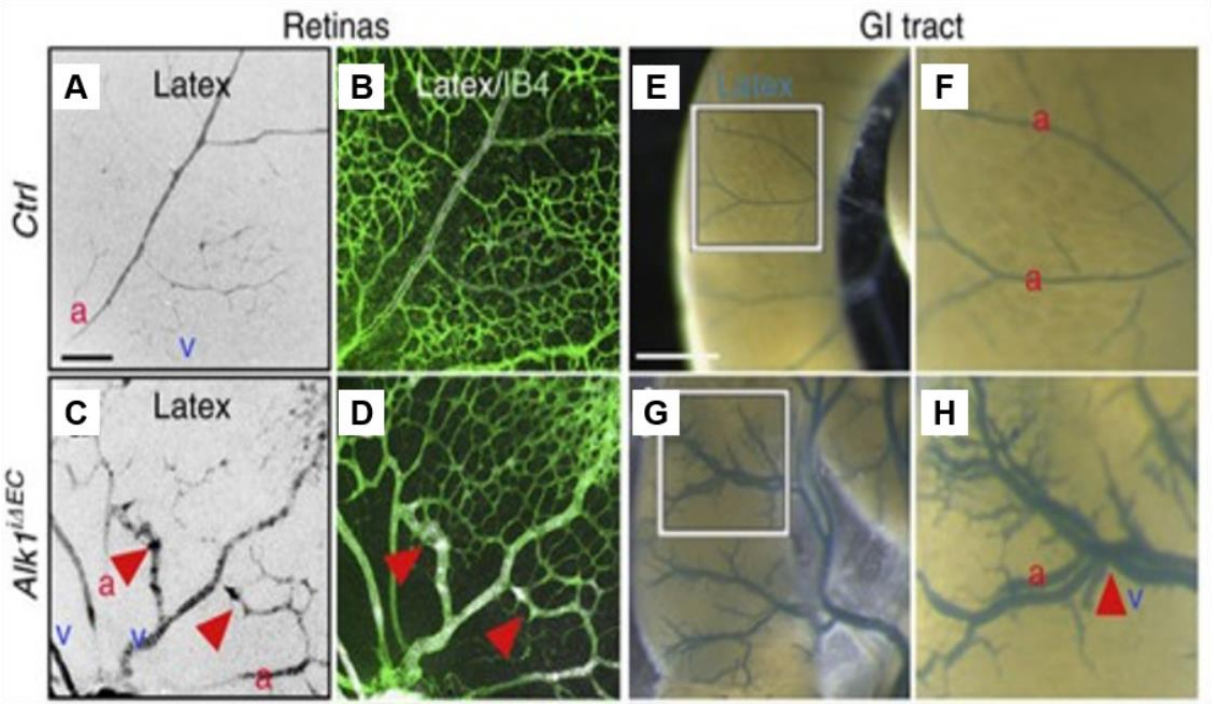

Figure 4: **EC-specific deletion of *Acvrl1* leads to AVM formation:** Staining of mouse retinas with either Latex dye or IB4 for control mice (A, B) and EC-specific *Acvrl1* knockout mice (C, D), red arrows indicate AVMs. Vascular staining of the small intestine in control (E, F) and tamoxifen-induced *Acvrl1* depletion (G, H), red arrows indicate latex-perfused veins. a: artery; v: vein. Adapted from [47].

1.3.3 *Smad4* Knockout Mouse Model

Smad4 depletion in ECs resembles the specific deletion of EC *Acvrl1,* resulting in the development of brain, lungs, and retinal AVMs during neonatal development. Malformations within the GI tract can be also observed [29, 40, 48]. This indicates that the *Smad4* model is more closely related to *Acvrl1* than *Eng* (Figure 5).

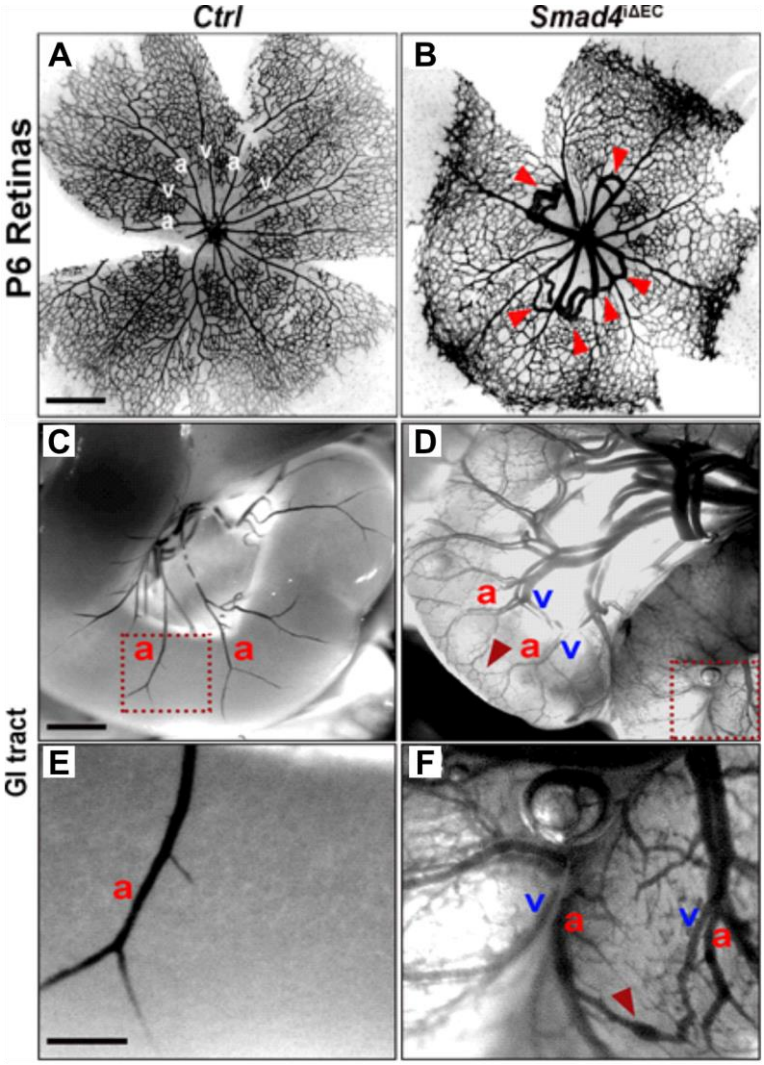

Figure 5: **Endothelial-specific deletion of *Smad4* leads to AVM formation:** Retinal staining from Control (A) and inducible *Smad4*-depletion (B), red arrows indicate AVMs. Vascular labeling of Control (C, E) and EC-specific *Smad4* deletion (D, F). Arrows indicate AVMs. Adapted from [29].

1.4 Role of blood flow in endothelial cells

ECs, which are located on the luminal surface of blood vessel walls, are continuously subjected to mechanical stimuli resulting from blood flow dynamics. The mechanical forces, specifically fluid shear stress (FSS) generated by perfusion, are crucial for modulating various physiological processes at the endothelial interface, triggering activation or inhibiting numerous signaling pathways essential for maintaining homeostasis and optimal vascular function [49].

FSS is critical for early vascular development in mice [50] and zebrafish [51] but also for homeostatic vessel remodeling in adult vasculature [52]. In vascular pathogenesis, FSS contributes to the initiation and progression of atherosclerosis [53]. Recent work has also implicated FSS in the vascular malformation pathogenesis of cerebral cavernous malformations (CCMs) [54] and AVMs [29, 47].

Blood flow within the circulatory system can be classified into laminar and turbulent flow. Laminar flow is characterized by blood's smooth and organized movement, which travels in parallel layers with minimal intermixing and creates laminar shear stress (LSS). This flow typically occurs in straight segments of blood vessels. Conversely, turbulent flow is defined by irregular and chaotic movement patterns, commonly occurring in areas with structural irregularities like bifurcations, branch points, and inner curvatures in blood vessels. This flow type leads to fluctuations in velocity and pressure within the bloodstream, responsible for oscillatory shear stress (OSS) [55-57].

The ECs react to these flow patterns via a junctional mechanosensory complex that includes platelet endothelial cell adhesion molecule 1 (PECAM1), vascular endothelial cadherin (VE-cadherin), and the VEGFA receptors, VEGFR2 and VEGFR3. Stimulation of this junctional complex by FSS or upon direct force on PECAM triggers activation of Src family kinases (SFKs) within seconds, resulting in ligand-independent activation of VEGF receptors and further downstream events, including PI3K/Akt and integrins activation. However, the mechanisms by which these proteins located at cell-cell junctions can sense forces from shear stress exerted on the apical surface are unclear. Within the junctional complex, VE-Cadherin acts as an adaptor protein. The VE-cadherin transmembrane domain is the critical VE-specific region required for the physical association of PECAM1 and VEGFRs and for subsequent activation of VEGFRs tyrosine kinases in response to FSS. PECAM1 was thought to be the true mechanosensor for many years, as the direct force applied to PECAM1 leads to the initiation of FSS cascades. Yet, recent work suggests that PECAM1 acts rather as a mecanotransducer within the junctional complex that requires an upstream event, presumably mediated by another mechanosensory component. The critical importance of FSS in cardiovascular development and function has driven intense investigation into the identification of mechanosensors, as they are the first responders to changes in the mechanical environment [56]. Several of these were recently identified, including Piezo1 [58], GPCRs (G- protein-coupled receptors) [59], or Plexin-Nrp1(Neuropilin-1)-Vegfr2 complex [60], among others. Yet, what are the functional EC mechanosensory whose disruption contributes to vascular malformations remain largely elusive.

This mechanosensory system converts mechanical stimuli into biochemical signals that will lead to changes in gene expression, the release of vasoactive substances, and cytoskeletal reorganization, which will ultimately initiate cellular responses [61, 62].

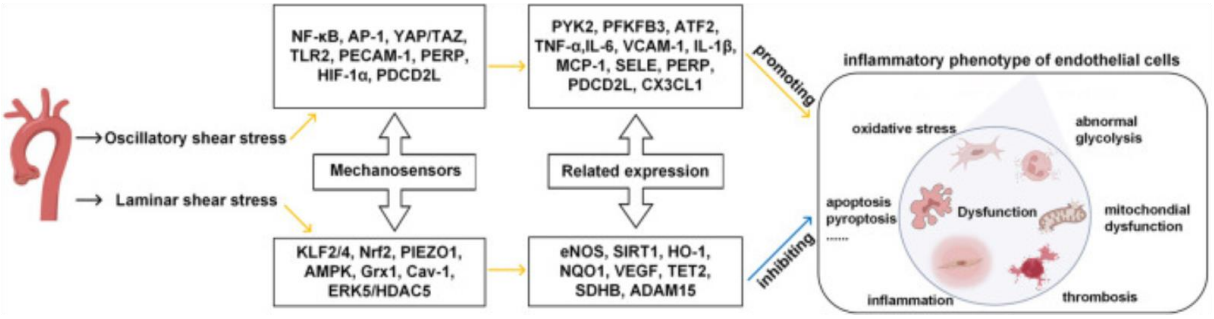

Figure 6: **Effects of different FSS patterns on EC function**: Representative image for flow patterns in the aorta. OSS occurs in the curvature. LSS occurs in the straight portion of the aorta. The yellow lines represent activation, while the blue line signifies inhibition. Adapted from [49].

LSS plays a critical role in vascular health by inhibiting the adhesion of monocytes and the proliferation of vSMCs [63]. Furthermore, LSS is conducive to promoting anti-inflammatory processes, evidenced by the upregulation of endothelial nitric oxide synthase (eNOS) [64], along with the transcription factors nuclear factor-E2-related factor 2 (Nrf2) [65], Krüppel-like factor 2 and 4 (KLF2/4) [66] and the activation of the serine/threonine kinase Akt [66]. In contrast, at regions such as the carotid bifurcation or aortic arch, there is a transition in blood flow patterns from LSS to OSS [67]. OSS is significantly correlated with microvascular and epicardial EC dysfunctions by additionally upregulating inflammatory cytokines and/or enhancing leukocyte adhesion to ECs [68, 69] (Figure 6).
KLF2 and KL4 transcription factors regulate more than 70% of the gene repertoire upon physiological (P)-FSS [70]. In CCMs, an aberrant upregulation of KLF2/KLF4 occurs through excessive Mitogen-Activated Protein Kinase Kinase/Extracellular Signal-Regulated Kinase 5 (MEKK2/3-ERK5) pathway activation due to disruption of MEKK3 from the CCM protein complex [71, 72]. ERK5 is also regulated upon P-FSS [73].

FSS influences various cellular responses, including EC number, fate, cell shape, and orientation (polarization). EC responses to FSS demonstrate specificity related to the particular vessel type and are governed by a distinct FSS set point. When P-FSS of high magnitude is near this set point, it fosters EC elongation and alignment parallel to the direction of flow, axial polarity (orientation of the ECs against the direction of FSS), concurrently inducing cell cycle arrest mediated arterial identity maintenance, thus contributing to vessel stabilization [74]. Under the physiological laminar flow of low magnitude, such as in capillaries, the ECs fail to align or to initiate polarity-induced migration [75-77]. This physiological response is mandatory to prevent EC regression in slowly perfused vessel beds [78]. P-FSS also maintains vessel diameter [79]. Changes in P-FSS patterns trigger transient or acute and adaptive EC remodeling of the vascular wall until the original FSS set point is restored. FSS that exceeds (high FSS, H-FSS) or falls below (low FSS, L-FSS) the FSS set point drives outward or inward remodeling, respectively [76, 80]. A chronic remodeling of vessels to reach the P-FSS set point will result in vascular instability and, ultimately to vascular disease.

1.5 Receptor Tyrosine Kinases in the Endothelium

Receptor tyrosine kinases (RTKs) represent a fundamental family that contains 58 members [81] of transmembrane proteins integral to cellular communication and signal transduction mechanisms [82]. These receptors, characterized by a single-pass transmembrane structure [83], are pivotal components of intracellular signaling pathways that govern diverse cellular processes, including proliferation, differentiation, metabolic regulation, and cellular motility [84].

RTKs initiate complex signaling cascades upon activation. Ligand binding induces receptor dimerization and trans-autophosphorylation, resulting in the phosphorylation of tyrosine residues located on the cytoplasmic tail of the receptor. These phosphorylated residues act as docking sites for various intracellular proteins that possess SH2 or PTB domains [85]. However, numerous reports emphasize that activation of RTKs may occur also in the absence of the ligand. The ligand-independent RTKs activation occurs either through pre-formed homo or hetero RTK dimers [86], activation via Copper-(II) ions [87], upon binding/activation to GPCRs [88], overexpression [89], mutations [90], formation of heterodimers [91], low-density lipoprotein (LDL) cholesterol [92] or upon FSS stimulation [93].

ECs express a plethora of RTKs with fundamental roles in vascular development, homeostasis, and vascular disease. The VEGFRs play a crucial role in angiogenesis, EC proliferation, migration, and survival [94]. While VEGFA displays the highest affinity for VEGFR1, activation of VEGFR1 receptor by phosphorylation is weak. Yet, VEGFR1 plays an anti-angiogenic role by acting as a decoy that controls the amount of VEGFA available to bind to and activate VEGFR2 [95]. VEGFR3 is required for embryonic and adult lymph angiogenesis. Upon VEGFC stimulation, VEGFR3–VEGFR2–NRP-1 complex formation mediates Akt activation, whereas ERK1/2 activation is primarily driven by VEGFR3 homodimers without contribution from NRP-1 or NRP-2, indicating that homo- or heterodimerization and the VEGF co-receptors can qualitatively and quantitatively modulate VEGFR signaling [96, 97].

The TIE (Tyrosine Kinase With Immunoglobulin Like And EGF Like Domains) 1 and TIE2 RTKs bind specifically to Angiopoietin ligands (ANG1–ANG4) and form an EC signaling pathway required for embryonic cardiovascular and lymphatic development. In adult vasculature, they are instrumental in regulating vascular stability and maturation [98]. ANG2 can function as a context-dependent agonist and antagonist of TIE [99]. Other RTKs expressed on endothelial cells include Platelet-Derived Growth Factor Receptors (PDGFRs) [100], Fibroblast Growth Factor Receptors (FGFRs) [101] and Ephrin receptors [99].

Activation of RTKs constitutes a complex signaling network that orchestrates EC behavior, angiogenesis, and vascular function through several downstream signaling pathways, including PI3K/Akt [102] and MAPK/ ERK signaling cascades [103]. The MAPK/ERK pathway

comprises two distinct pathways leading to the activation of ERK1/2 and ERK5, respectively [104, 105] (Figure 7). RTK signaling in ECs occurs at the plasma membrane and intracellularly after endocytosis, enabling spatiotemporal regulation of signaling events [106].

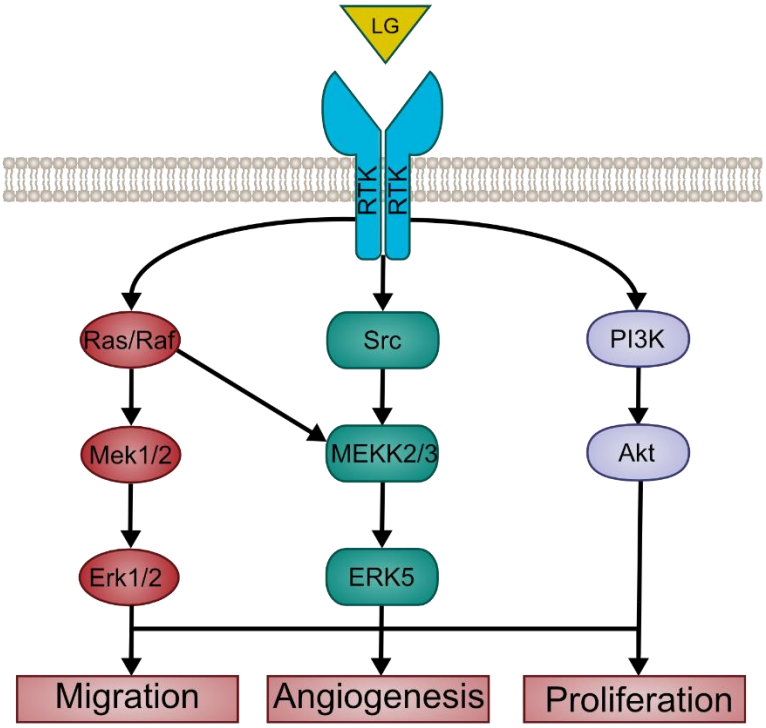

Figure 7: **RTK signaling in ECs:** The RTKs undergo dimerization and subsequent transphosphorylation upon ligand binding. This process facilitates the recruitment of various intracellular signaling proteins. The activation of two different MAPK signaling cascades is mainly mediated by Erk1/2 or Erk5. PI3K is recruited to activate RTKs, which subsequently activates Akt signaling. All three pathways are essential for EC migration, angiogenesis, and proliferation.

1.6 Molecular mechanisms of AVM formation

The synergistic interaction between BMP9/BMP10 and FSS is crucial in promoting and maintaining EC quiescence and vascular homeostasis. Significantly, P-FSS stimulates the Alk1-Eng receptor complex formation, a mechanism that results in augmented activation of Smad1/5/9 in ECs stimulated with a low concentration of BMP9 [107]. This mechanism explains how canonical BMP9 signaling is maintained active in mature vessels wherein the concentration of secreted BMP9 is reduced. Conversely, canonical SMAD4 signaling is required for FSS-mediated upregulation of pericyte recruitment factors and FSS-induced cell cycle arrest [107, 108]. Furthermore, in zebrafish and neonatal mouse models, AVMs form in regions of high flow, emphasizing the implication of mechanosensing in AVM pathogenesis. Mechanistically, AVMs result from the overactivation of the PI3K/Akt signaling pathway in ECs, and inhibition of excessive PI3K/Akt blunted AVM formation in several mouse models of HHT [109]. Increased Akt activation was further confirmed in HHT patients [110].

Interestingly, the same signaling hub is downstream of FSS. P-FSS initiates the activation of the PI3K/Akt signaling pathway, which is critical in orchestrating a range of downstream responses under physiological conditions. These responses include cell survival, cellular alignment, and vasodilation [111]. The pivotal role of PI3K in the FSS response is closely associated with its essential functions in the signaling pathways downstream of various RTKs like VEGFR2, VEGFR3, and TIE2 [112, 113]. Physiological levels of SMAD15 activation are also required for Akt induction upon P-FSS, as excessive BMP9 blocks the effect of FSS on Akt phosphorylation [29].

Blockage of either PI3K/Akt [47], VEGFA-VEGFR2 [114], mTOR (mammalian Target of Rapamycin) in combination with VEGFR2 [115], or ANG2-Tie2 [116] rescues AVM formation. However, the relationship between P-FSS-mediated EC responses, BMP9/10 signaling, and the PI3K/Akt signaling pathway remains poorly understood and warrants further scientific investigation.

2. Aim of the study

Disruption of SMAD4 signaling in ECs results in augmented PI3K/Akt-mTOR pathway activation due to transcriptional increase in CK2-mediated PTEN hyperphosphorylation. Inhibition of VEGFR2-PI3K/Akt-mTOR signaling by pharmacological approaches prevents, improves, or rescues AVM formation in HHT animal models. Additionally, the physiological activation of the PI3K/Akt-mTOR pathway represents a critical regulatory node downstream of physiological FSS that is also regulated upon the BMP9/10 signaling pathway. How BMP9 signaling restricts FSS-mediated PI3K signaling to maintain EC quiescence remains an open question.

Therefore, my PhD thesis will:

1.) address the role of FSS-mediated activation of PI3K/Akt signaling node in AVM pathogenesis
and
2.) identify the SMAD4-mediated regulatory events upstream of FSS that are required to maintain EC quiescence.

3. Results

3.1 Augmented KLF4 leads to hyper-responsiveness to FSS in cells with SMAD4 loss of function (LOF)

3.1.1 SMAD4 restricts the FSS induced KLF4 activation in vitro

To elucidate the dysregulated players induced by FSS in the context of loss of SMAD4, I conducted bulk RNA sequencing (RNA-seq) comparing human umbilical vein endothelial cells (HUVECs) treated with a control siRNA (*CTRL siRNA*) and a specific *SMAD4* siRNA to induce SMAD4 knockdown (*SMAD4KD*) grown in static versus subject to physiological FSS (P-FSS) at 12 DYNES/cm² for 24 hours. Among all differentially expressed genes upon FSS, *KLF4* was within the first 10 genes whose expression was augmented upon *SMAD4KD* (Figure 8A). As KLF4 functions as a mechanosensor activated by FSS and is crucial in regulating various shear-responsive genes [117], I further focused on identifying its role in AVM pathogenesis. To validate the RNA sequencing findings, I performed quantitative real-time polymerase chain reaction (RT-PCR) on *SMAD4* siRNA HUVECs in comparison with *CTRL* siRNA subject to a gradient of shear stress (1-5-12 DYNES/cm²) for 2 hours. The RT-PCR results validated the *SMAD4* siRNA in inducing *SMAD4* depletion (Figure 8B) and an increased threshold of *KLF4* activation with the shear stress magnitude upon FSS in *SMAD4KD* HUVECs, thereby confirming the RNA sequencing data (Figure 8C). These findings indicate that SMAD4 restricts flow-induced KLF4 activation irrespective of FSS magnitude, thereby contributing to the maintenance of EC quiescence.

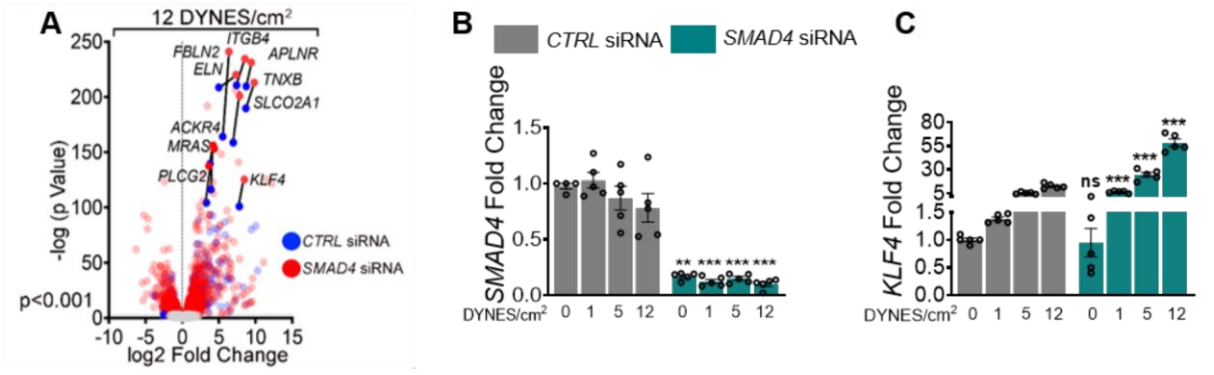

Figure 8: **SMAD4 restricts flow-induced activation of KLF4:** (A) Volcano plot illustrating the top 10 genes that are significantly upregulated after 24 hours of exposure to 12 DYNES/cm² in *CTRL* and *SMAD4*-depleted HUVECs (n=3 per group). *SMAD4* (B) and *KLF4* (C) mRNA expression after exposure to 1, 5, and 12 dynes for 24 hours (n=5). Data is shown as mean ± SEM. One-way ANOVA was used for statistical testing. *P<0.05, **P<0.01, ***P<0.001, ns: non-significant.

3.1.2 Validation of RNA-seq Data in vivo

FSS levels exhibit their peak within the developing retinal plexus, particularly near the optic nerve, subsequently diminishing toward the advancing sprouting front. To validate the restrictive role of SMAD4 in FSS-induced Klf4 activation in vivo, dissected retinas from postnatal day 6 (P6) tamoxifen-induced *Smad4* fl/fl and *Smad4*$^{i\Delta EC}$ mice were immunolabelled for KLF4 and Isolectin B4 (IB4) to visualize the vasculature. In control *Smad4* fl/fl retinas, KLF4 expression was minimal in the low FSS vascular front and capillary ECs (Figure 9A). Moderate levels were observed in medium FSS veins, while the highest expression was determined in high FSS arteries, particularly at the first retinal branch points where AVMs frequently develop [29]. In contrast, retinas from *Smad4*$^{i\Delta EC}$ mice demonstrated a marked increase in Klf4 expression in the AVMs, reaching the highest peak expression levels in ECs within the AVM, compared to the associated feeding arteries or veins (Figure 9C-D). Reduced Klf4 intensity was noted in the arteries and veins located upstream of the AVMs or in vessels non-engaged in AVM formation, corroborating recent observations indicating lower flow dynamics outside of AVMs [118].

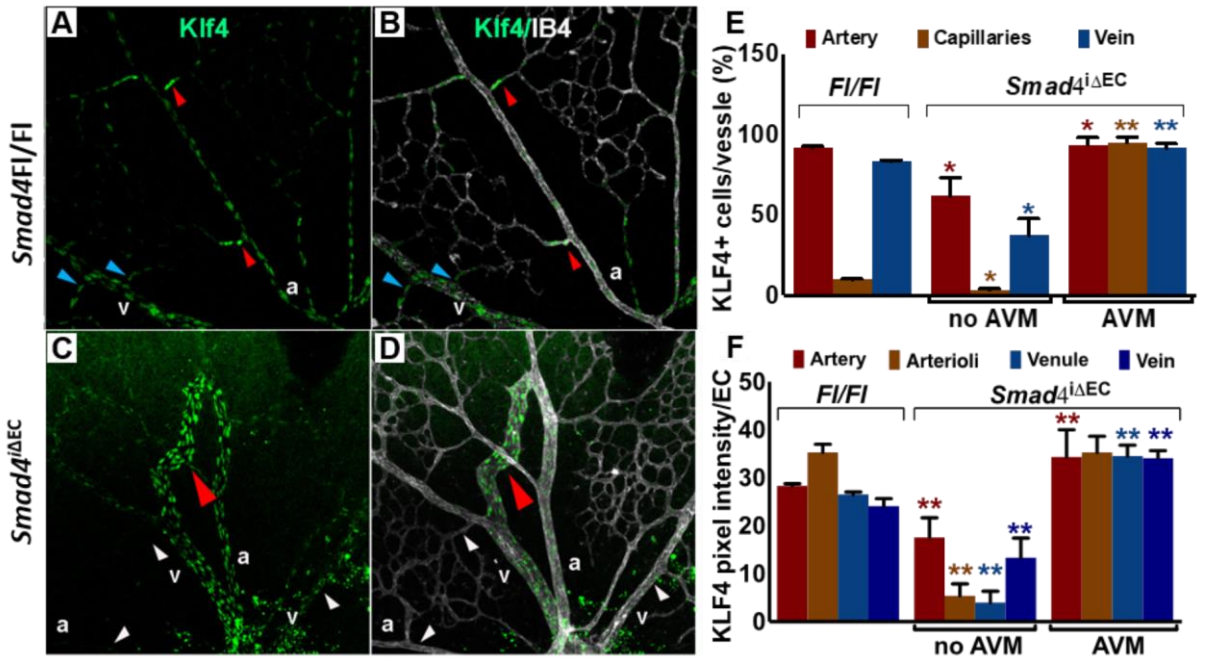

Figure 9: **FSS-induced Klf4 defines AVMs:** A-D Immunofluorescence labeling of Tx-induced P6 retinas from *Smad4* fl/fl and *Smad4*$^{i\Delta EC}$ mice with Klf4 (green) and IB4 (white). Red arrows in A and B show branch points in arteries with high Kff4 expression, whereas blue arrows point towards branch points in veins with low Klf4 expression. Red arrows in C and D indicate the AVM. The ratio of Klf4 positive cells per vessel length is shown in (E), and the respective pixel intensity in (F) (n=6). Experiments performed by Ms. Kuheli Banerjee. Data represented as mean ± SEM. One-way ANOVA was used for statistical testing. *P<0.05, **P<0.01, ***P<0.001, ns: non-significant a: artery; v: vein.

3.1.3 High flow-induced KLF4 is a pivotal factor in the formation of AVMs

To further investigate the role of Klf4 in the pathogenesis of AVMs, we (myself and Kuheli Banerjee) employed an in vivo model to assess AVM formation. Therefore, a transgenic double knockout (Ko) mouse line was created by crossing *Klf4* fl/fl with *Smad4*$^{i\Delta EC}$ mice to generate a genetic model of tamoxifen (Tx) EC-inducible double Ko *Smad4*;*Klf4*$^{i\Delta EC}$ mice. These mice were injected with Tx at P0-P2 (Figure 10A), and retinal analysis was conducted at P6. Notably, the inactivation of *Klf4* effectively reduced AVM formation in *Smad4*$^{i\Delta EC}$ retinas (Figure 10B-D); interestingly, loss of *Klf4* did not rescue the significant sprouting observed at the vascular front. These findings suggest that flow-induced Klf4 plays a specific role in the FSS-mediated AVM pathogenesis.

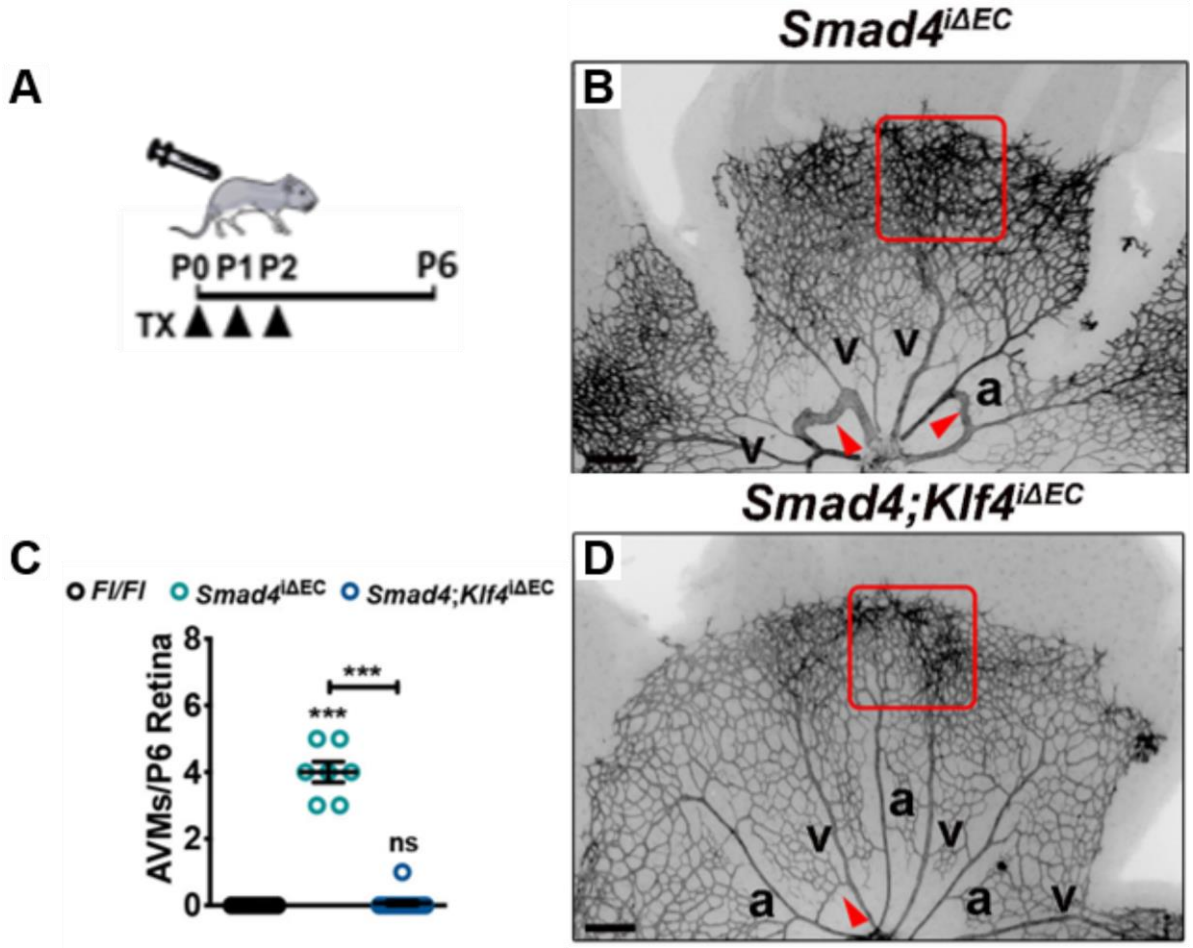

Figure 10: **Klf4 inactivation rescues AVM formation:** Schematic of the strategy used for intragastric Tx injection (A). Vasculature labeling with IB4 of P6 retinas from *Smad4*$^{i\Delta EC}$ (B) and *Smad4*;*Klf4*$^{i\Delta EC}$ (D) mice, red arrows indicate AVMs. Quantification of the AVM number (C). Experiments conducted by Ms Kuheli Banerjee. Data is shown as mean ± SEM. One-way ANOVA was used for statistical testing. *P<0.05, **P<0.01, ***P<0.001, ns: non-significant. a: artery; v: vein

3.1.4 FSS-induced excessive KLF4 is a PI3K/Akt upstream event

Upregulation of PI3K/AKT signaling following the inactivation of the BMP9/10 - Alk1- Smad4 signaling pathway contributes to the pathogenesis of AVMs and increased sprouting angiogenesis [29]. In the context of P-FSS, the activation of the PI3K/Akt pathway plays a critical role in modulating EC responses. To test whether KLF4 acts up- or downstream of PI3K/Akt signaling, we (Kuheli Banerjee) inhibited PI3K signaling in HUVECs using Pictilisib, followed by an evaluation of *KLF4* activation post-2-hour exposure to P-FSS via RT-PCR. The results revealed no significant alteration in KLF4 activation due to PI3K inhibition (Figure 11A), indicating that flow-induced KLF4 activation does not depend on PI3K signaling. To assess whether KLF4 operates upstream of PI3K signaling, I measured pAkt in static versus 2 hours of P-FSS conditions upon depletion of *KLF4* or *SMAD4* alone or in combination *KLF4;SMAD4* by Western blot. Quantification of Western blot results indicated that FSS-induced Akt activation is contingent upon *KLF4* in static ECs, with *KLF4* depletion leading to the normalization of Akt hyperactivation in *SMAD4KD* HUVECs (Figure 11B, C).

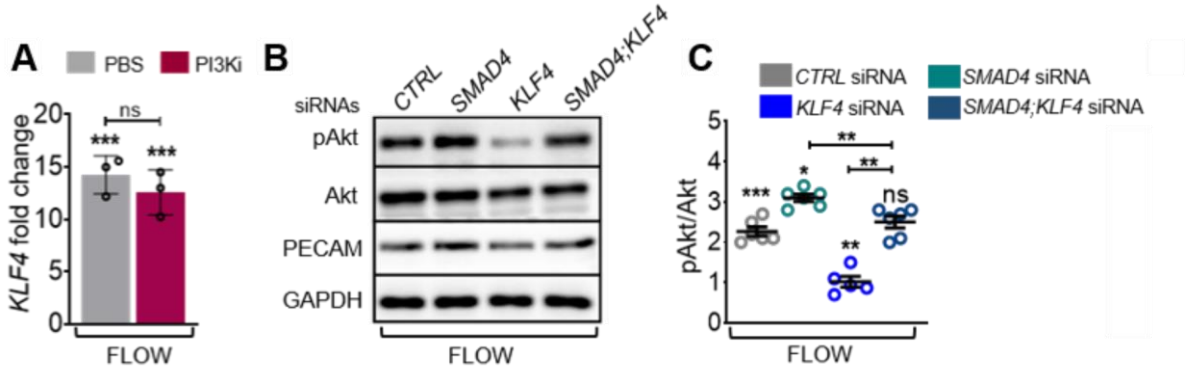

Figure 11**: FSS-induced excessive KLF4 operates upstream of PI3K/AKT signaling:** mRNA expression level of *KLF4* in HUVECs treated with PI3Ki pictilisib and subjected to 12 DYNES/cm^2 (n=3) (A). Western blot for pAkt, Akt, PECAM, and GAPDH in CTRL, SMAD4, KLF4, or *SMAD4*;*KLF4* transfected HUVECS subjected to 12DYNEs/cm2 for 2 hours (B). Experiments performed by Ms. Kuheli Banerjee. Quantification of pAkt (n=6) levels (C). Data is shown as mean ± SEM. One-way ANOVA was used for statistical testing. *P<0.05, **P<0.01, ***P<0.001, ns: non-significant.

3.1.5 TIE2 is Essential for KLF4-Mediated Akt activation in response to FSS

Since KLF4 has emerged as a key regulator of the PI3K/Akt signaling pathway, although the precise underlying mechanisms remains unclear. I hypothesized that KLF4 mediates the activation of Akt in response to FSS by transcriptionally controlling an upstream direct regulator of the PI3K/Akt cascade. To test this hypothesis, I analyzed RNA-seq data comparing static conditions with samples subject to a 12 DYNES/cm² shear stress in HUVECs and focused on potential PI3K/Akt pathway regulators. Specifically, I considered TEK Receptor Tyrosine Kinase (*TEK*, which encodes TIE2), *FLT4* (encoding VEGFR3), and *KDR* (coding for VEGFR2), as well as *CD31* (coding for PECAM-1), established activators of PI3K/Akt, but also *PTEN*, a negative regulator of PI3K signaling.

The heatmap analysis (Figure 12A) revealed that both *FLT4* and *TEK* were significantly upregulated under P-FSS, while *KDR* and *PTEN* were downregulated, and *CD31* expression remained unchanged. To validate these results and further investigate the FSS-dependent regulation of these genes upon *KLF4*, I conducted RT-PCR on HUVECs with *KLF4* depletion in both static and 2-hour P-FSS conditions. RT-PCR data indicated a significant increase in *TEK* expression and a reduction in *PTEN* levels in *CTRL* cells subjected to P-FSS, whereas *FLT4* and *CD31* exhibited no substantial changes (Figure 12B). Interestingly, *KLF4* deletion did not alter the expression levels of *FLT4* and *PTEN*; moreover, while the deletion decreased the protein levels, it did not significantly alter the *CD31* gene expression. Thus, *TEK* was the sole gene whose upregulation in response to FSS was KLF4 dependent.

To elucidate whether *KLF4* directly regulates *TEK*, I further assessed *TEK* expression in cells overexpressing *KLF4 (KLF4OE)* using RT-PCR analysis. The *KLF4OE* cells exhibited a marked increase in *TEK* expression (Figure 12C). Consequently, *TEK* was selected for further investigation as a potential modulator of flow-induced PI3K signaling downstream of KLF4.

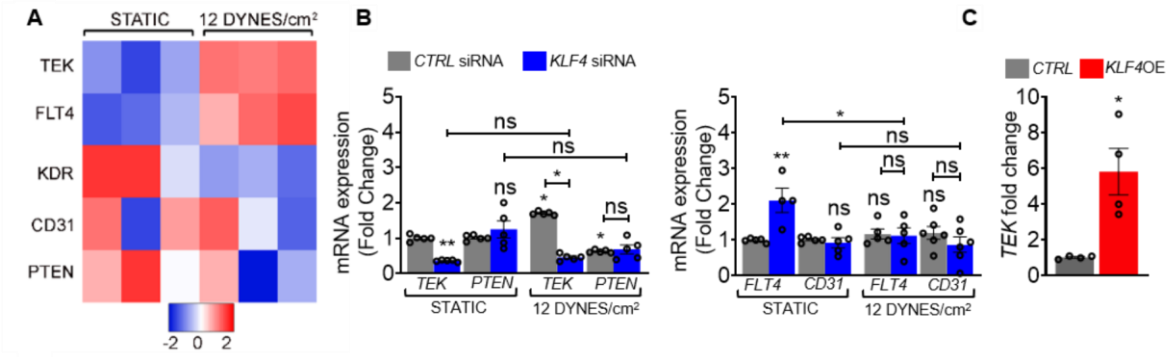

Figure 12: **FSS-mediated upstream regulators of the PI3K/Akt signaling pathway:** Heatmap for potential PI3K/Akt signaling mediators (n=3). The color key shows the Row Z-score. mRNA expression for *TEK* and *PTEN* (left panel) and *FLT4* and *CD31* (right panel) in *CTRL* and *KLF4*-KO HUVECs (n=5) (B). RT-PCR analysis of *TEK* in *CTRL* and *KLF4OE* cells (n=4). Data is shown as mean ± SEM. One-way ANOVA was used for statistical testing. *P<0.05, **P<0.01, ***P<0.001, ns: non-significant.

Previously published ChIP (chromatin immunoprecipitation) sequencing data from pulmonary arterial endothelial cells (PAECs) with a constitutively active *MEK5* as a stimulator of *KLF4* demonstrated an enrichment of *KLF4* at the active enhancer region within the *TEK* gene [119] (Figure 13A), suggesting a direct role in transcriptional regulation. To validate the requirement of *TEK* in KLF4-mediated Akt signaling, *TEK* was deleted in *CTRL* versus *KLF4OE* HUVECs subject to FSS for 2 hours. The deletion of *TEK* resulted in a significant loss of pAkt levels, both in *KLF4OE* cells and in response to flow-induced conditions. These findings indicate that *TEK* is a direct transcriptional target of KLF4, and TIE2 downstream of KLF4 is required for Akt activation in the context of FSS (Figure 13B, quantification shown in Figures 13C and D).

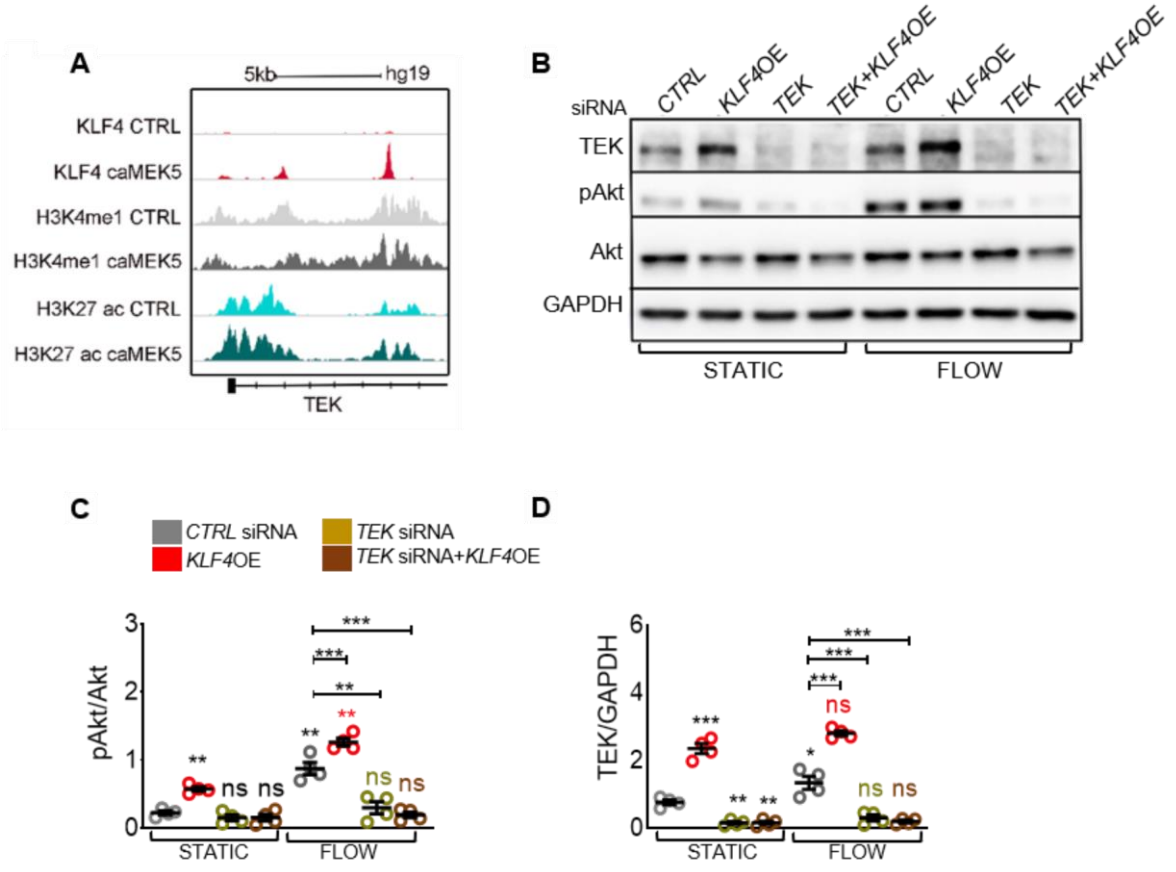

Figure 13: **TIE2 is required to activate Akt signaling:** Reanalysis of previous published ChIP-Seq of KLF4 overexpressing (caMEK5) PAECs (A) showing the genomic region of *TEK* with integrative genomics viewer (IGV). Two distinct peaks within the enhancer region of *TEK* were identified in the *KLF4OE* cells. WB analysis of TEK, pAkt, Akt and GAPDH on *CTRL*, *KLF4OE*, *TEK* and *KLF4OE*;*TEK* siRNA HUVECs (B). Quantification of pAkt (C) and TEK(D) protein levels. Ms. Kuheli Banerjee performed WB experiments. Data represented as mean ±SEM. One-way ANOVA was used to determine statistical significance. *P<0.05, **P<0.01, ***P<0.001, ns: non-significant.

3.2 Identification of Klf4 upstream regulatory mechanisms in AVM pathogenesis

3.2.1 RNA-seq reveals RTKs as potential regulators of FSS-induced KLF4

To identify potential regulators upstream of FSS-induced excessive Klf4-Akt activation in the AVM pathogenesis, I performed bulk RNA sequencing from ECs isolated from Tx-induced P6 *Smad4* fl/fl and *Smad4*$^{i\Delta EC}$ retinas. Gene ontology (GO) analysis indicated a significant overrepresentation of GO terms associated with EC motility, blood vessel formation, and extracellular matrix organization. Conversely, the downregulated genes exhibited enrichment for genes involved in the transcriptional regulation of P53 and mitosis-related cell cycle processes (Figure 14A).

Upon validation of the RNA sequencing data through immunolabeling in developing retinas, I observed significant differential regulation of several genes in AVMs compared to non-AVM vasculature. The RNA sequencing analysis identified upregulation of the Delta Like Canonical Notch Ligand 4 (*Dll4*) gene and downregulation of *Tek* (Figure 14B) genes. Upon labeling, the expression of the two genes could be validated; the Dll4 was increased, and Tie2 decreased in mutant retinas. However, their expression patterns were entirely reversed in AVMs (yellow arrows Figure 14C). These findings indicate differential gene expression within the FSS-mediated AVMs and non-AVM regions and imply that bulk RNA sequencing is not viable for identifying AVM-specific differential gene expression.

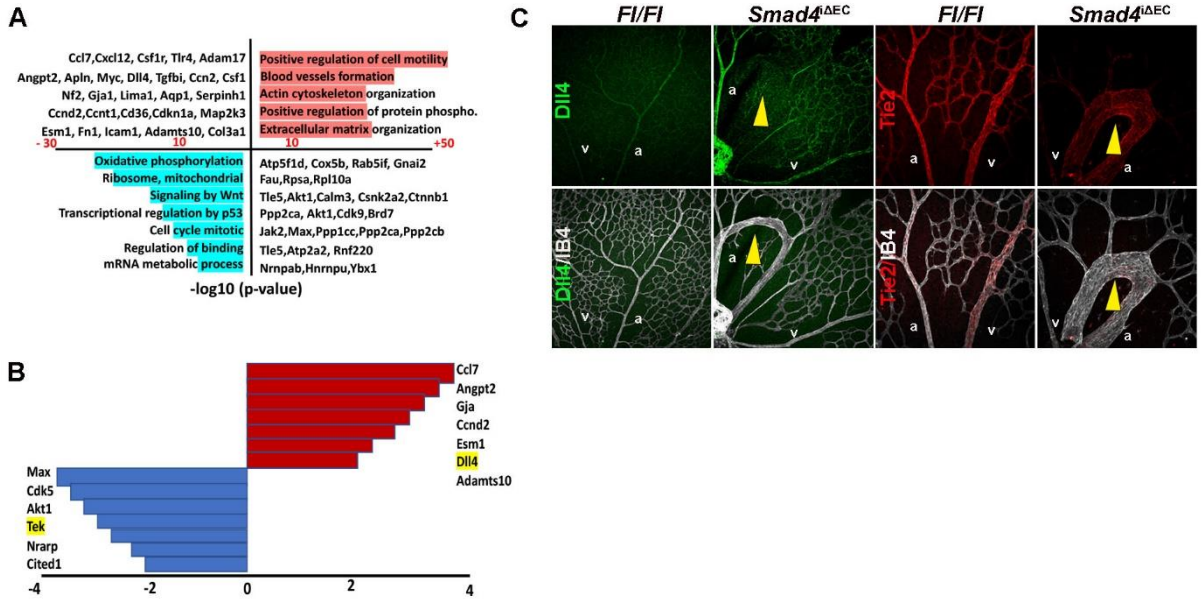

Figure 14: **SMAD4-dependent gene expression repertoire:** Representative genes and enriched GO terms in upregulated versus downregulated genes upon *Smad4* depletion in retinal ECs (A), n=3, log 2-fold change, *P<0.05. Graph showing the most upregulated and downregulated genes in retinal ECs upon *Smad4* depletion (B). Labeling of Tx-induced P6 *Smad4* fl/fl and *Smad4*$^{i\Delta EC}$ retinas for Dll4 (green), Tie2 (red), and IB4 (white). Yellow arrows mark AVMs (C). a artery, v vein.

Since the RNA sequencing from the P6 retinas could not identify mediators of KLF4-induced hypersensitivity within the AVMs, I performed bulk RNA sequencing on HUVECs treated with either a control siRNA (si*CTR*) or an *SMAD4* siRNA (si*SMAD4*) and subject cells to varying magnitudes of FSS (ranging from 0 to 12 dynes/cm^2 for 2 hours (Figure 15A). Principal component analysis (PCA) revealed a clear separation between the si*CTRL* and si*SMAD4*-treated groups, with the variance increasing in response to higher FSS levels (Figure 15B).

GO analysis from the differential expressed genes (comparison of all groups between si*CTR* and si*SMAD4*) revealed, as expected, several *SMAD4*-related terms, including “blood vessel development” and “cell migration,” both of which are pertinent to EC biology and their

response to mechanical forces such as shear stress. Interestingly, GO analysis also identified RTK signaling as a significant differential expressed pathway (Figure 15C).

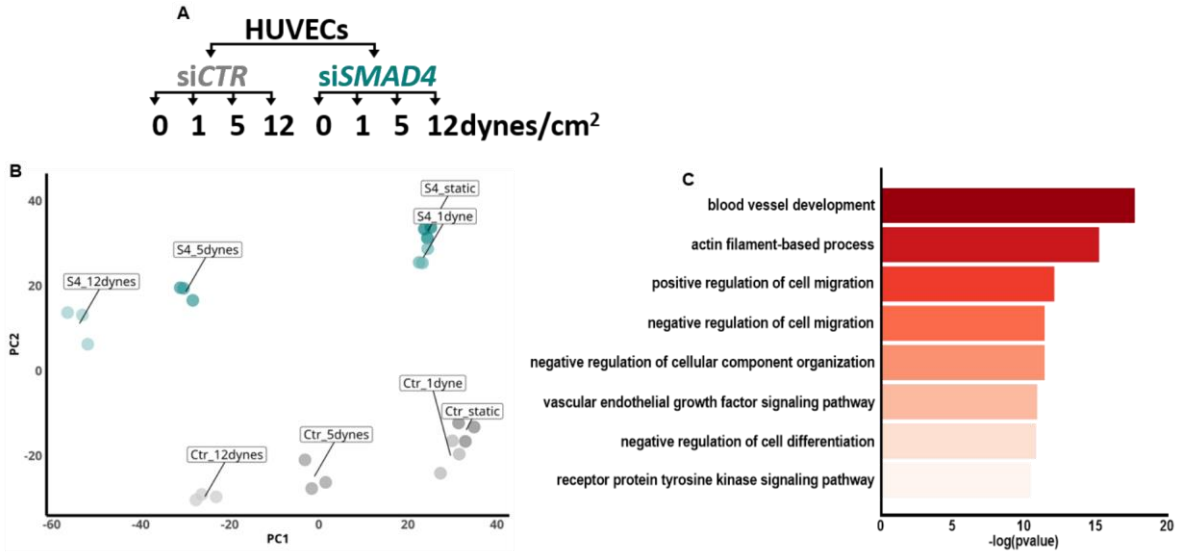

Figure 15: **RNA-seq reveals RTKs as potential FSS hypersensitivity inducers:** Schematic of the strategy used for RNA sequencing (A). PCA plot showing the characteristics of the samples (B). GO analysis comparing the si*CTR* versus the si*SMAD4* groups (C).

To further investigate the putative role of RTKs in AVM pathogenesis, I have examined the top five differentially expressed RTKs in all conditions. The heatmap (Figure 16A) showed an apparent upregulation of all 5 RTKs upon *SMAD4* depletion in static cells. In FSS conditions in *CTRL siRNA* cells, TIE1, KDR, Fibroblast Growth Factor Receptor 1 (FGFR1), and Discoidin Domain Receptor Tyrosine Kinase (DDR) 1 exhibited similar expression patterns, being downregulated only in low FSS conditions. On the other hand, *KIT*, a type III RTK for stem cell factor (SCF), was downregulated by FSS irrespective of the FSS magnitude. SMAD4 loss blocked the effect of FSS-mediated downregulation of TIE1, KDR, FGFR, and *DDR1* at low FSS magnitudes and of KIT at all FSS magnitudes, yet with a decreasing trend from low to high FSS magnitude (Figure 16A). These findings are further visualized with the Ridgeplot in (Figure 16B).

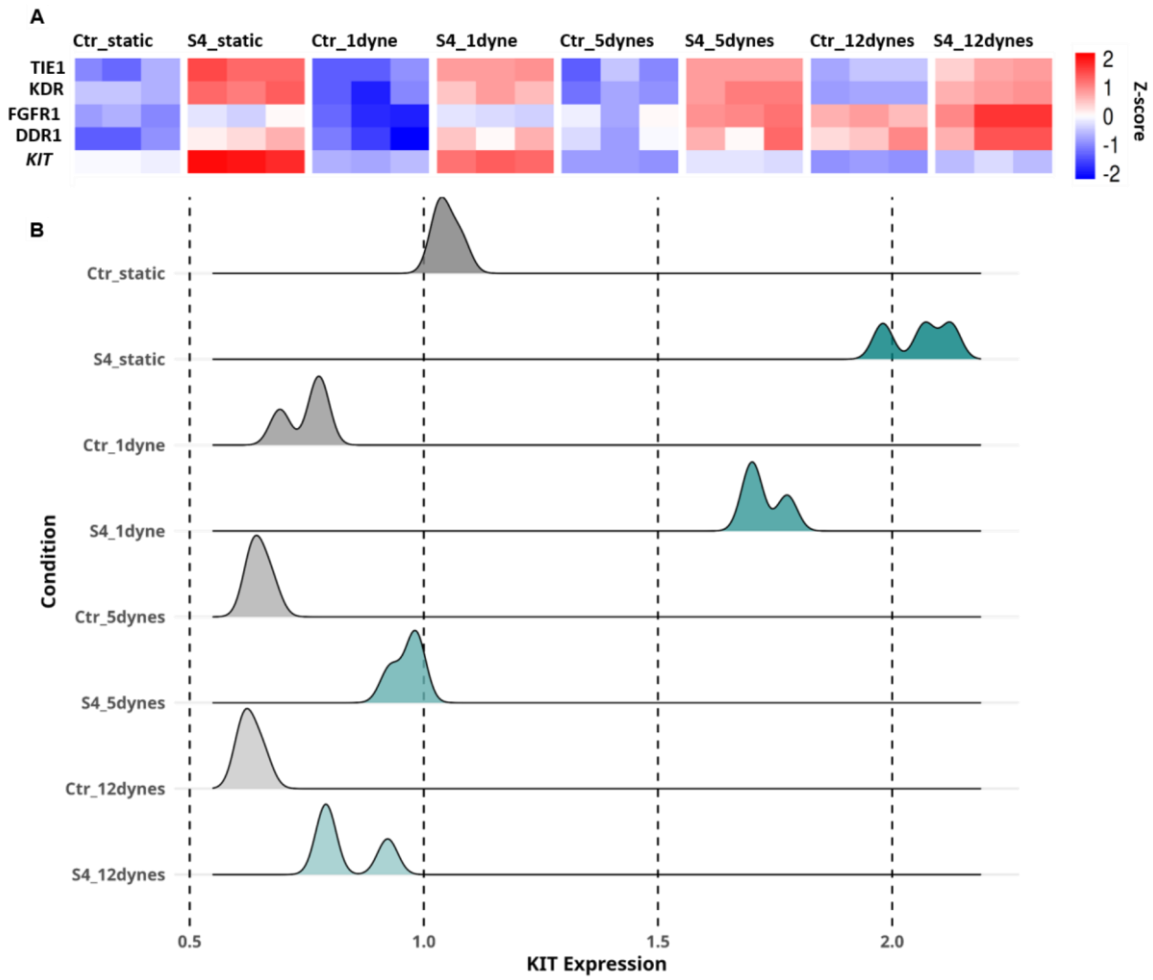

Figure 16: **Analysis of RTK expression upon loss of *SMAD4*:** Heatmap from the normalized reads of the TOP5 differentially expressed RTKs in the RNA-seq dataset (A). Ridgeplot of the gene expression data from *KIT* in the RNA-seq dataset (B).

As retinal AVMs form in regions of high FSS and we have identified that Smad4 regulates the FSS set point [108], I further wanted to evaluate the most relevant FSS conditions to AVM pathology. Computational blood flow simulations were performed (by Prof. Dr. Fatemeh Mirzapour, Technische Universität Darmstadt) on P6 *Smad4* fl/fl and *Smad4*$^{i\Delta EC}$ retinas. Figures 17A and 17B depict the selected regions for the computational simulation. The simulated wall shear stress (WSS) within the AVM area (Figure 17D) was notably lower compared to the control retina (Figure 17C), with WSS values confined to a range between 1 and 5 Pascal (Pa). These results indicate an altered mechanical environment within the AVM region. Remarkably, the pattern of simulated WSS closely resembles the expression profile of *KIT* (Figure 16B) more than any other of the top five RTKs in the RNA-seq dataset. This suggests that the abnormal shear stress in the AVM region may influence the expression of *KIT*, which could be a critical mediator of the altered vascular responses in AVM pathogenesis.

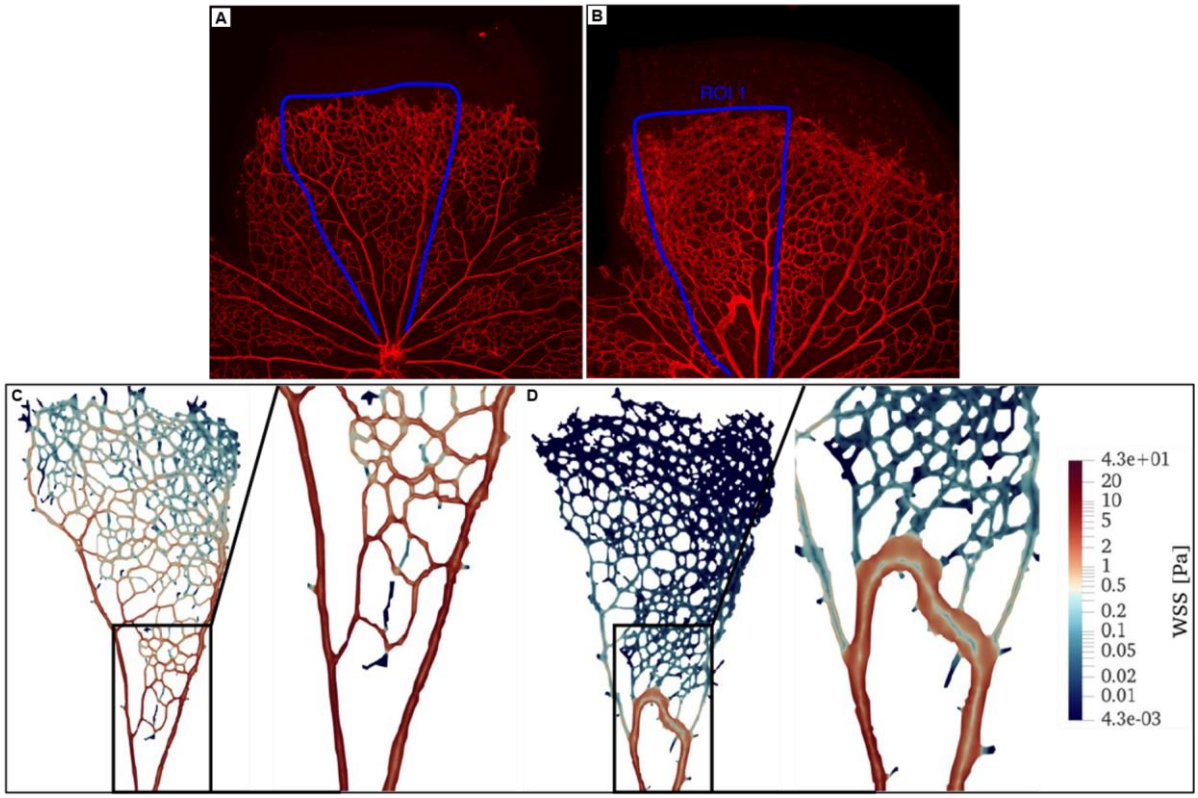

Figure 17: **Image-based Blood Flow Simulation in the retinal vasculature:** Regions used for flow simulation in a *Smad4* fl/fl retina (A) and a *Smad4*$^{i\Delta EC}$ retina (B) are marked in blue color (A). Blood flow simulation in the *Smad4* fl/fl retinas (C) and the *Smad4*$^{i\Delta EC}$ (D) shear stress levels are indicated in WSS levels. Prof. Dr. Fatemeh Mirzapour performed the simulations.

3.2.2 BMP9-SMAD4 is required for FSS-mediated KIT inhibition

To validate my findings in RNA-seq data sets, I performed RT-PCR for *KIT* in the same experimental set-up. HUVECs depleted for si*CTRL* versus si*SMAD4* were subject to 1, 5, and 12 dynes/cm of FSS for two hours (Figure 18A). The RT-PCR results confirmed the RNA sequencing data, showing significant downregulation of *KIT* irrespective of the FSS magnitude in *siCTRL* cells. *SMAD4KD* blocked this effect, with a decreasing trend from low towards high FSS magnitude. These results are thus paralleling the trends observed in computational simulations.

To further confirm the RNA seq and the RT-PCR data and, at the same time, to focus on the regulation of KIT in physiological conditions, I performed Western blot in static versus 12 dynes/cm^2 FSS (Figure 18 D and 18E) in si*CTRL* versus si*SMAD4* HUVECs. Results confirm the downregulation of KIT upon FSS and its upregulation upon *SMAD4* depletion. Interestingly, *SMAD4KD* completely blocked the effect of FSS on KIT downregulation. Thus, taken together, these results suggest that KIT expression is not solely regulated at the transcriptional levels, but rather post-transcriptionally mechanisms may interfere with potential alterations in protein stability, phosphorylation, or translation as previously identified [120] in response to shear stress and *SMAD4KD*.

To further investigate the potential regulation of *KIT* by BMP9 signaling, HUVECs were stimulated with 10ng/ml BMP9 in addition to FSS (Figure 18B). RT-PCR analysis revealed that *KIT* expression was significantly downregulated upon BMP9, and BMP9 treatment further augmented the FSS-mediated inhibition of *KIT*, indicating a synergistic effect of BMP9 and FSS on *KIT* downregulation.

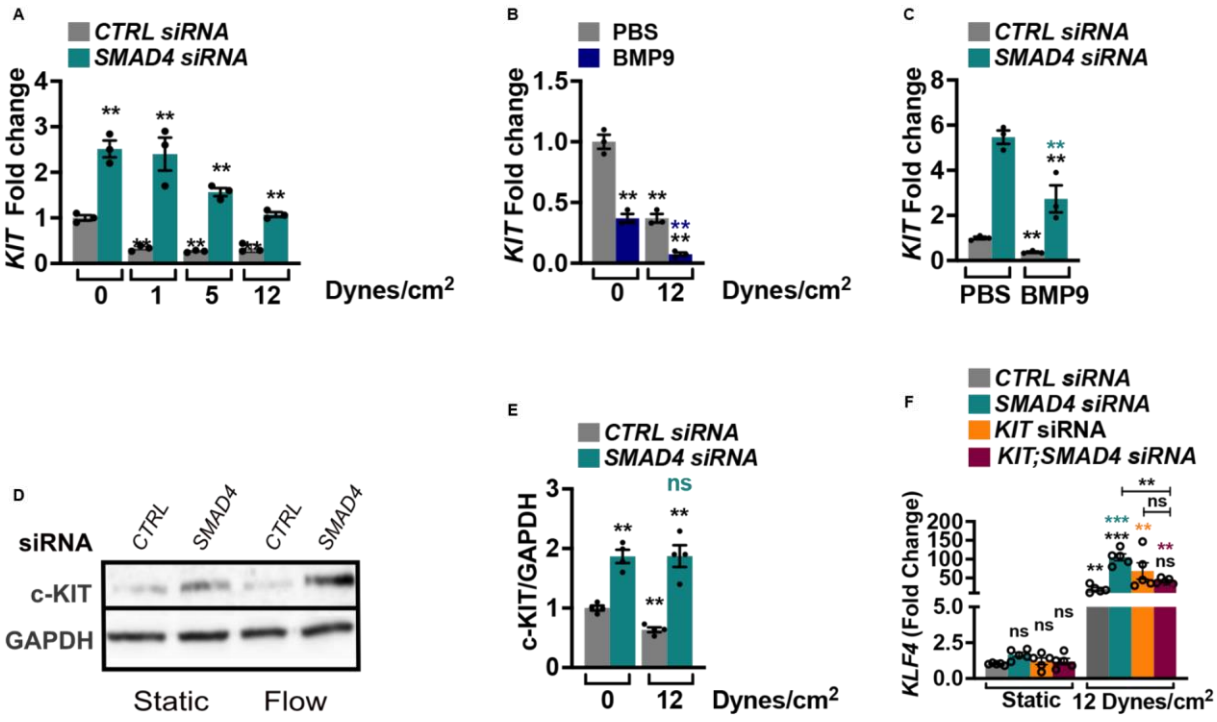

Figure 18: **SMAD4 signaling is required for FSS-mediated inhibition of KIT expression:** RT-PCR on HUVECs subjected to 1, 5, and 12 dynes/cm for 2 hours, treated with *CTRL* or *SMAD4* siRNA. RNA expression of HUVECs treated with 1 ng/ml of BMP9 and subjected to static or 12 dynes/cm^2 (B). RT-PCR on HUVECs transfected with either *CTRL* or *SMAD4* siRNA and treated with either PBS or 1ng/ml BMP9 for 2 hours (C). WB from CTRL and SMAD4-KD HUVECs subjected to static or 12 dynes/cm^2 for 2 hours (C) and the quantification of the KIT protein expression normalized to GAPDH (E). mRNA expression of HUVECs transfected with either, *CTRL*, *SMAD4*, *KIT* or *SMAD4*;*KIT* siRNAs grown in static or subject to 12dynes/cm^2 for 2 hours. Data represented as mean ±SEM. One-way ANOVA was used to determine statistical significance. *P<0.05, **P<0.01, ***P<0.001, ns: non-significant.

To further assess the regulation of *KIT* upon canonical BMP9 signaling pathway, si*CTRL* and si*SMAD4* HUVECs were treated with 10ng/ml of BMP9 or phosphate-buffered saline (PBS) for 2 hours (Figure 18C). RT-PCR analysis revealed that BMP9-mediated *KIT* inhibition was partially dependent on SMAD4, thus indicating additional mechanisms implicated in *KIT* regulation.

To further explore the implication of KIT in EC mechanotransduction, I transfected HUVECs with siRNAs targeting *SMAD4*, *KIT*, and a combination of both and subjected the cells to 12 dynes/cm2 FSS and measured *KLF4* modulation upon FSS (Figure 18F). As expected, FSS-induced *KLF4* expression in siCTRL cells and FSS-induced *KLF4* expression was further exacerbated upon *SMAD4KD*, thus confirming findings in Figure 8B. Interestingly, *KIT*

depletion alone did not interfere with FSS-induced *KLF4* activation. Yet *KIT* loss of function (LOF) significantly normalized *KLF4* induction in *SMAD4KD* upon FSS to si*CTRL* levels. These results suggest that FSS-mediated *KIT* downregulation is required to maintain physiological *KLF4* activation. Thus, loss of SMAD4 blocks the inhibitory effect of FSS on *KIT,* resulting in excessive RTK expression and presumably activation and exacerbated *KLF4* induction upon FSS.

3.2.3 FSS-induced Erk5 activation is KIT-dependent

As activation of KIT regulates several downstream signaling pathways in ECs, including MAPK and PI3K/Akt pathway, I performed WB analysis to examine the activation of these pathways under static and FSS conditions. HUVECs were transfected with *siCTRL,* si*SMAD4*, si*KIT*, and a combination of both, si*SMAD4* and *KIT,* and subject to FSS conditions. The blots were probed for phosphorylated ERK1/2, ERK5, and Akt to assess downstream pathways' activation (Figure 22A).

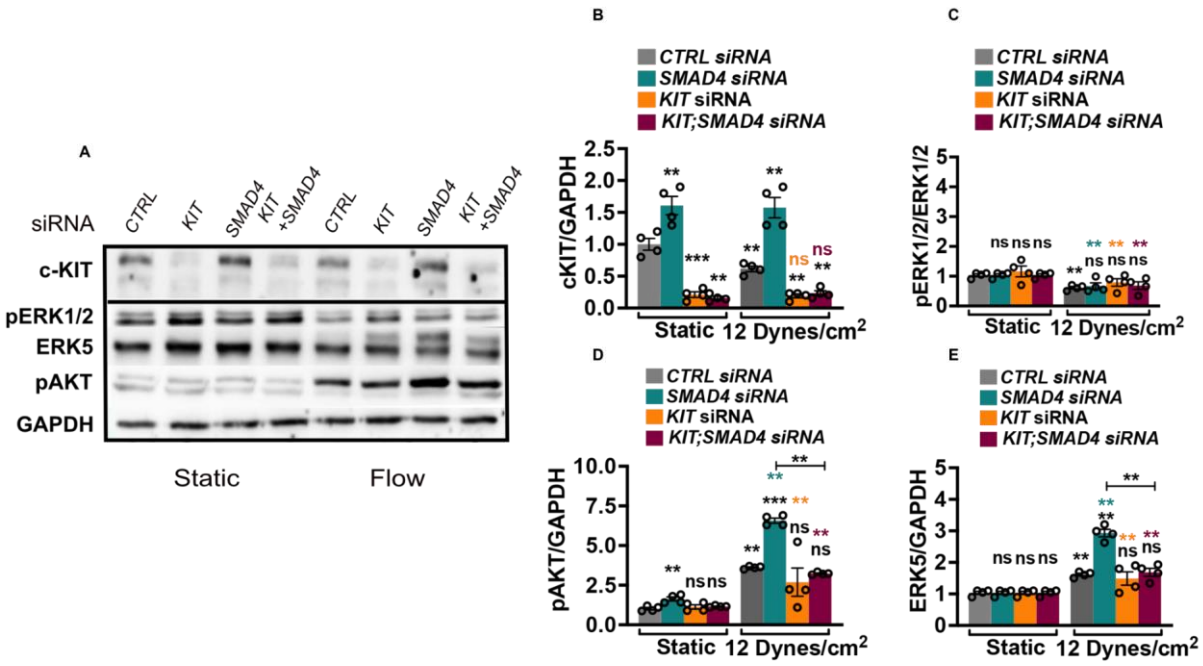

Figure 19: **FSS-induced Erk5 activation is downstream of KIT:** WB for KIT, pERK1/2, ERK5, pAkt, and GAPDH of HUVECs transfected with siRNAs for *CTRL*, *KIT*, *SMAD4* or *KIT*;*SMAD4* and subjected to FSS levels of 0 or 12 dynes/cm^2 for 2 hours (A). Respective normalized quantifications for KIT (B), pERK1/2 (C), pAkt (D), and ERK5 (E) protein levels. Data is shown as mean ±SEM. One-way ANOVA was used to determine statistical significance. *P<0.05, **P<0.01, ***P<0.001, ns: non-significant.

The results confirmed KIT protein downregulation upon *KIT* knockdown (Figures 19A and 19B), confirming successful siRNA-mediated *KIT* depletion. While SMAD4 loss did not interfere with FSS-mediated ERK1/2 phosphorylation (Figure 19C), ERK5 and pAkt were excessively activated in *SMAD4*-deficient cells under FSS conditions (Figure 19 D, E).

Interestingly, depletion of *KIT* in *SMAD4KD* cells normalized the excessive activation of ERK5 (upper band) and of Akt upon FSS without any effect in *siCTRL*. These findings highlight the implication of KIT in modulating ERK5 and AKT signaling only in pathological conditions, such as SMAD4 LOF.

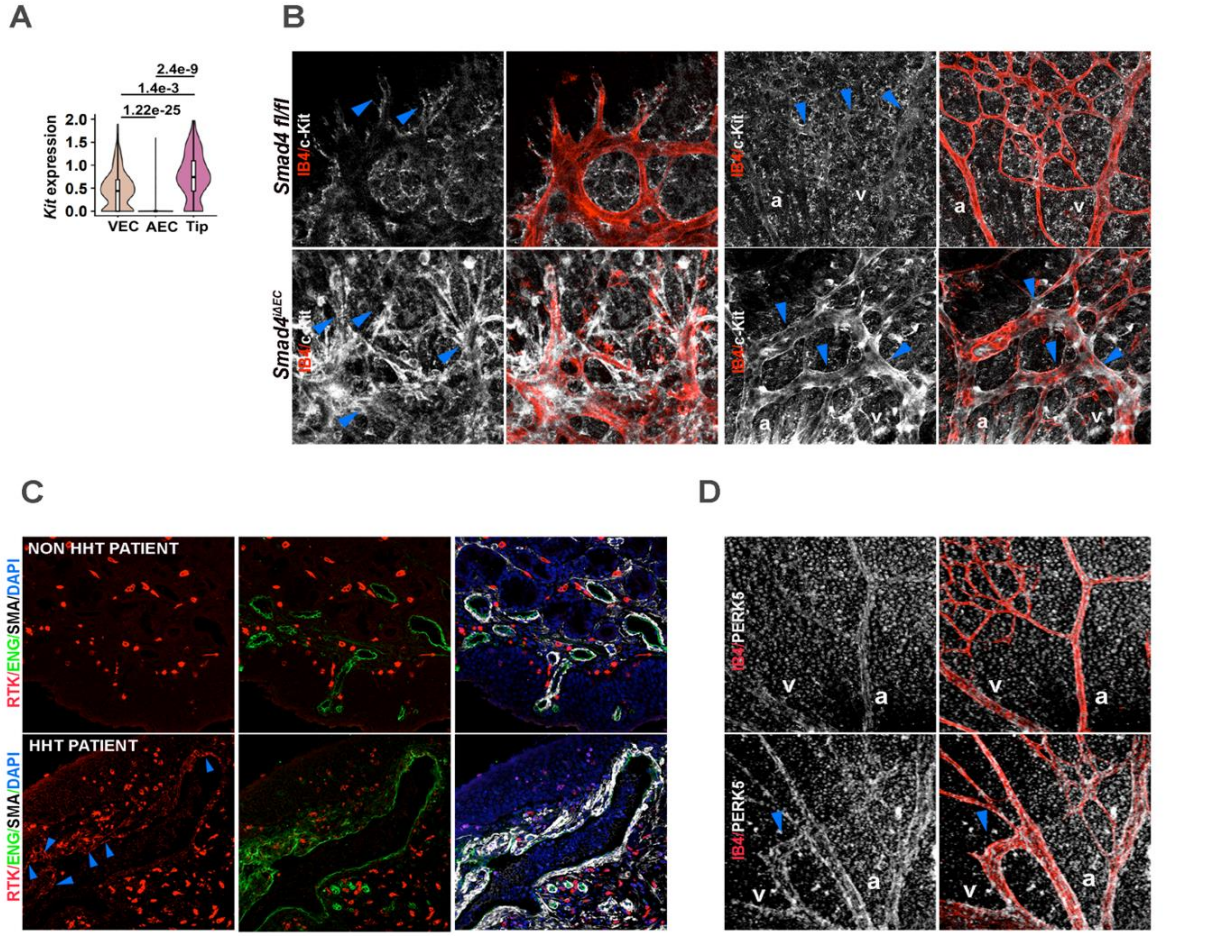

Figure 20: **Kit expression in SMAD4 HHT mouse model:** Reanalysis of Kit expression from previously scRNA-seq published in P6 wild type retinas [121]. Kit (white) and IB4 (red) immunofluorescence staining on *Smad4* fl/fl and *Smad4*$^{i\Delta EC}$ mouse P6 retinas (B), blue arrows indicate Kit expression in the tip versus vein and capillaries. IF staining of Human HHT samples from the nasal mucosa in a non-AVM area and AVM C) with DAPI (blue), SMA (white), ENG (green), and KIT (red). Blue arrows show KIT-positive areas within the vasculature. pERK5 (white) and IB4 (red) immunofluorescence staining of P6 Tx induced *Smad4* fl/fl and *Smad4*$^{i\Delta EC}$ retinas (D), blue arrow indicates AVM. Venous EC (VEC), arterial EC (AEC), and endothelial Tip cells (Tip). a: artery; v: vein

To confirm these findings in vivo, tamoxifen-induced P6 *Smad4* fl/fl and *Smad4*$^{i\Delta EC}$ retinas were immunolabelled for Kit (white) and IB4 (red) (Figure 20B). Low Kit was detected in the tip, vein, and venous capillaries in control retinas, thus confirming *Kit* expression in single-cell RNA-seq data from P6 wild-type retinas (Figure 20A). In *Smad4*$^{i\Delta EC}$ retinas, Kit was upregulated in all retina regions, including the tip cells, arteries, veins, and AVMs. To confirm these findings also in HHT patients, I labeled skin biopsies from HHT2 patients versus control donors. Interestingly, Kit was upregulated within the AVMs, while in non-AVM patients, the

endothelium was entirely negative for KIT (Figure 20C). I also confirmed the increased activity of Erk5 in the retinas by labeling for a pErk5 antibody (white) and IB4 (red) (Figure 20D). These observations further support the relevance of KIT upregulation in AVM pathology, providing evidence that the mechanisms observed in the experimental models may apply to human disease. Thus, taken together, these results suggest that an increase in Kit-mediated Erk5 activation characterizes AVMs.

To investigate whether other BMP9/10 signaling pathway components similarly affect *KIT* expression and the downstream Erk5 and Akt activation, I performed RT-PCR and WB analysis in *ALK1* and *SMAD1/5* LOF cells using siRNA strategy. Depletion of either *ALK1* or *SMAD1/5* led to downregulation of *KIT* expression in a similar pattern as in *SMAD4*-deficient cells (Figure 21A).

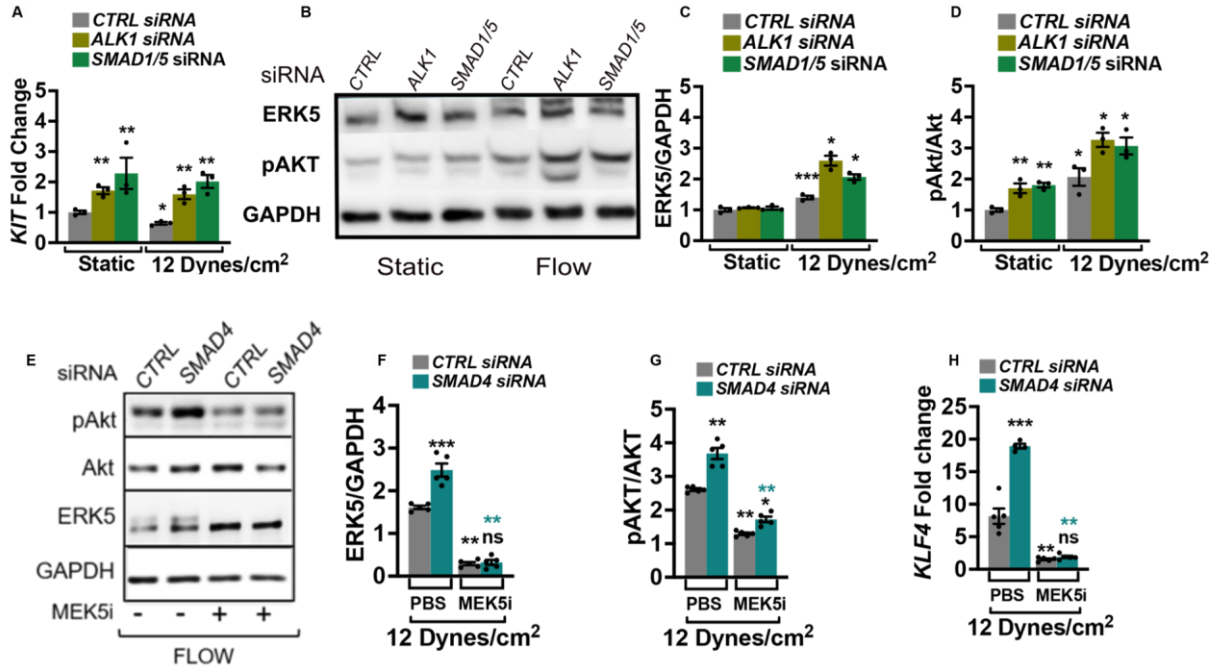

Figure 21: **ERK5 is required for FSS-induced KLF4 expression: RT-PCR analysis for KIT on CTRL, ALK1,** or *SMAD1/5* knockout HUVEVCs subjected to static or 12dynes/cm^2 for 2 hours(A). WB for pAkt, pAkt, ERK5, and GAPDH of HUVECs transfected with siRNAs for CTRL, ALK1, or *SMAD1/5* and subjected to FSS for 2 hours(B). Quantification of WB for ERK5(C) and pAkt(D). WB from CTRL and *SMAD4*-KD HUVECs subjected to static or 12 dynes/cm2 for 2 hours and either treated with 5µM BIX02189 or PBS for 3 hours (E). Respective normalized quantifications for ERK5(F) and pAkt(G). *KLF4* mRNA expression from RT-PCR analysis on HUVECs on the same conditions(H). Data is shown as mean ± SEM. One-way ANOVA was used for statistical testing. *P<0.05, **P<0.01, ***P<0.001, ns: non-significant.

Through WB analysis, I further assessed the phosphorylation levels of pAkt and ERK5 in *ALK1* and *SMAD1/5* LOF cells (Figure 21B-D). The results showed a similar pattern of activation as observed following *SMAD4KD*. Specifically, pAkt and ERK5 were upregulated in both *ALK1* and *SMAD1/5* LOF cells upon FSS, mirroring the changes in *SMAD4KD* cells. This supports

the hypothesis that disruption of BMP9/10 signaling components, such as *ALK1, SMAD1/5*, or SMAD4, leads to similar alterations in key signaling pathways, confirming that KIT regulation is part of a conserved mechanism across multiple AVM models.

To investigate the involvement of ERK5 in *KLF4* regulation, I treated *siCTRL* versus *siSMAD4* cells with BIX02189, a MEK5/ERK5 inhibitor (MEKi), to block the signaling upstream of ERK5, and subject cells to P-FSS. Western blot analysis revealed that FSS-induced ERK5 and pAkt were downregulated upon MEKi treatment in both the control and *SMAD4KD* cells (Figure 21 E-G). Additionally, qPCR analysis (Figure 21G) showed that *KLF4* expression was downregulated in both conditions upon MEKi treatment, further supporting the role of ERK5 in regulating KLF4 and the downstream Akt activation in normal versus pathological conditions. These findings suggest that FSS-mediated KLF4-Akt activation is downstream of ERK5.

3.2.4 Induction of ERK5-KLF4 via KIT is ligand-independent

To investigate whether the overactivation of Akt and KLF4 upon FSS in SMAD4 LOF HUVECs is a ligand-dependent or independent event, I performed WB analysis on HUVECs treated with 50 ng/ml SCF for 15 minutes in both *CTRL* and *SMAD4KD* cells under static and FSS conditions (Figure 2A). Interestingly, exogenous SCF augmented Akt activation in both *siCTRL* and si*SMAD4* cells (Figure 22B); however, SCF did not affect ERK5 activation levels (Figure 22C), suggesting that ERK5 activation occurs independently of the ligand.

To further validate this finding, I performed RT-PCR analysis for *KLF4*. I found that *KLF4* expression did not significantly change upon SCF treatment for 2 hours (Figure 22D), neither in *CTRL* siRNA nor in *SMAD4* siRNA HUVECs, reinforcing the idea that the ERK5-KLF4 activation upon FSS does not implicate the ligand.

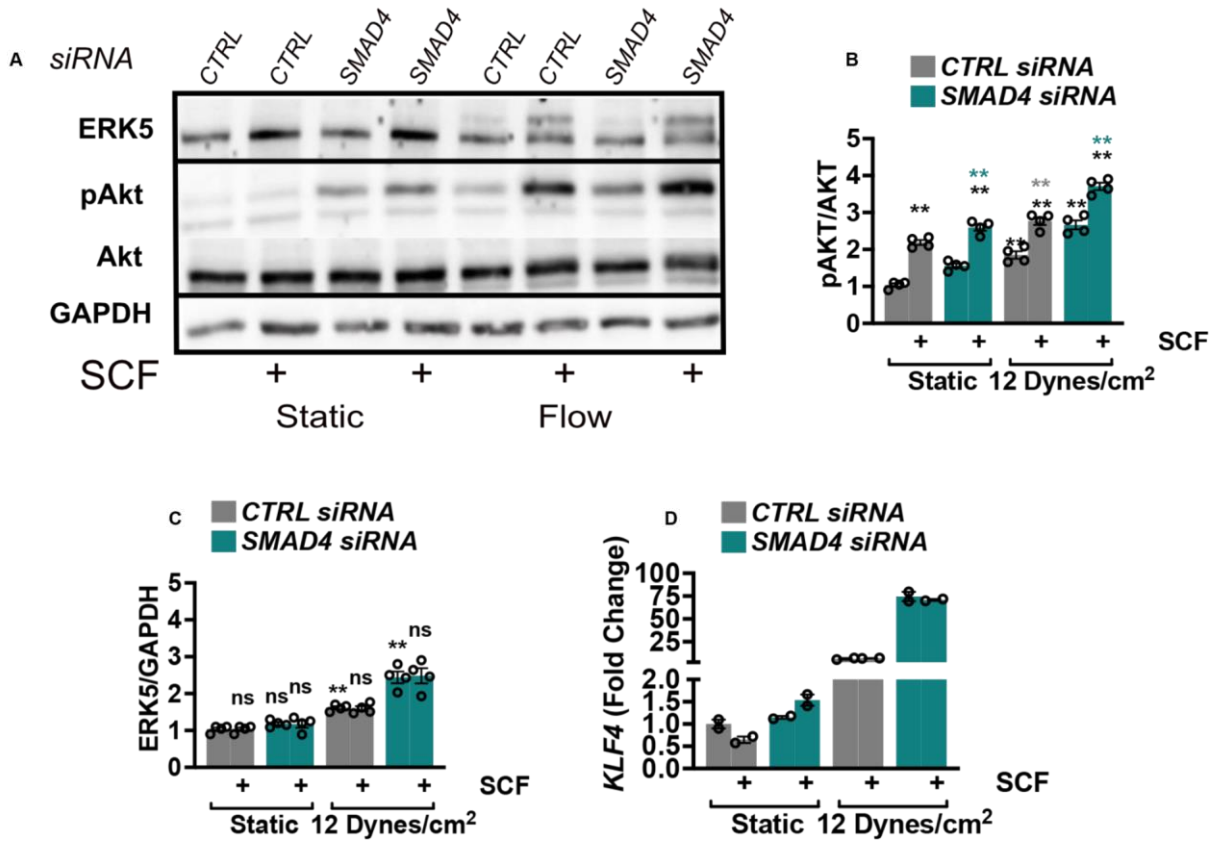

Figure 22: **Induction of ERK5-KLF4 via KIT is ligand-independent:** WB for ERK5, pAkt, Akt, and GAPDH of HUVECs transfected with siRNAs for *CTRL* or *SMAD4*, subjected to 12dynes/cm^2 for 2 hours further treated with PBS or 50ng/ml for 15 minutes(A). Respective normalized quantifications for pAkt (B) and ERK5 (F). *KLF4* mRNA expression from RT-PCR analysis on HUVECs on the same conditions. Data is shown as mean ± SEM. One-way ANOVA was used for statistical testing. *P<0.05, **P<0.01, ***P<0.001, ns: non-significant. a: artery; v: vein

3.2.4 Inhibition of KIT rescues AVM formation

To further investigate the potential therapeutic role of Kit inhibition in AVM pathology, I first screened in vitro for the most efficient KIT inhibitor that can reduce ERK5 and Akt activation. HUVECs transfected with siRNA as control and siRNA *SMAD4* were subject to P-FSS and treated for 4 hours with already described inhibitors: c-Kit-IN-5-1 (100nM), Masitinib (600nM), and Imatinib (900nM) in comparison with DMSO. Through WB analysis, I tested the efficiency of these drugs in rescuing FSS-mediated ERK5 and Akt activation upon *SMAD4* depletion. WB analysis revealed that none of the drugs significantly affected ERK5 or Akt activation in si*CTRL* HUVECs. However, in SMAD4 siRNA cells, Masitinib was the best drug targeting ERK5 activation and downstream Akt activation.

Considering the specificity of Masitinib in inhibiting ERK5 activation, I tested the in vivo efficacy of Masitinib to rescue AVM pathogenesis. *SMAD4* fl/fl and *SMAD4*$^{i\Delta EC}$ neonates in a mixed mTmG background (Gfp+ ECs show recombination) were treated with Tx to induce gene depletion at P1-P3, and Masitinib was injected at 50ug/g at P5 and P6. Retinas were dissected and immunolabeled for IB4 (red) and GFP (green). Quantification of the number of

AVMs revealed that masitinib efficiently rescued the number of AVMs in *SMAD4*$^{i\Delta EC}$ without affecting the vascular density at the sprouting front. These results indicate that KIT inhibition could be a promising novel approach for treating AVM-related vascular abnormalities.

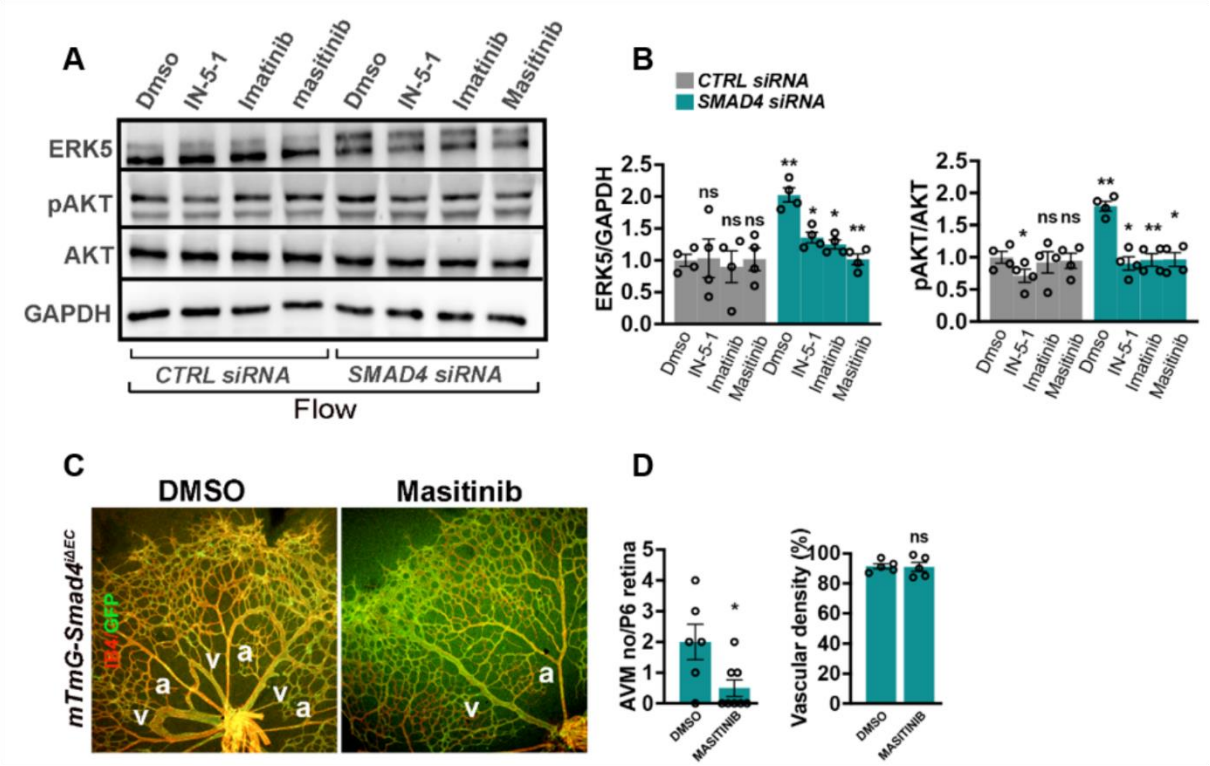

Figure 23**: Inhibition of KIT rescues AVM formation:** WB for ERK5, pAkt, Akt, and GAPDH of HUVECs transfected with siRNAs for *CTRL* or *SMAD4* treated with DMSO, c-Kit-5-IN-1 (100nM), Masitinib (600nM), or Imatinib (900nM) for 4 hours and subjected to 12dynes/cm^2 for 2 hours (A). Quantification of ERK5 and pAkt levels (B). Immunofluorescence labeling of Tx-induced P6 retinas from *Smad4*$^{i\Delta EC}$ mice injected with DMSO or Masitinib (C). The vasculature is marked with IB4 in red. The total amount of AMVs per retina (n=8) and vascular density (n=5) are quantified in (D). Data represented as mean ± SEM. One-way ANOVA was used for statistical testing in (B), and Student's T-test was used in (D). *P<0.05, **P<0.01, ***P<0.001, ns: non-significant. a: artery; v: vein

In summary, in the first part of my thesis, in close collaboration with my lab member, Kuheli Banerjee, we identified that SMAD4 restricts FSS-mediated KLF4 induction to temper the PI3K/Akt signaling activation in ECs, with TIE2 being essential for KLF4-mediated Akt activation. This novel mechanism is also required for FSS-mediated EC quiescence. In the second part of my thesis, I identified KIT as the upstream regulator of KLF4-TIE2-pAkt by employing RNA sequencing. In healthy endothelium, BMP9-SMAD4 signaling restricts FSS-induced KIT upregulation to maintain physiological ERK5 activation, which is a KLF4 upstream event. These findings underscore the role of FSS-mediated KIT inhibition and its downstream signaling pathways in AVM pathogenesis and highlight potential therapeutic targets for AVM treatment. How KIT-mediated ERK activation and how KIT can contribute to AVM pathogenesis in a ligand-independent manner are further questions to be addressed.

4. Discussion

AVMs are abnormal connections between arteries and veins. Thus, the capillary bed bypass leads to complications such as stroke, brain abscess, hypoxemia, or vessel rupture, depending on their location and stage, with treatment options ranging from surgical intervention to embolization and radiation, alongside additional therapies for smaller or inoperable AVMs. The absence of pharmacological approaches for AVM treatment highlights significant gaps in our understanding of their pathogenesis. Clinical trials in HHT patients with the anti-VEGF antibody Bevacizumab [122], the anti-angiogenic inhibitor Thalidomide [123], or the multi-RTK inhibitor Pazopanib [124] showed an improvement in recurrent epistaxis, infusion dependency or complete blood count (CBC) parameters. However, these treatments did not show a promising therapeutic outcome for AVM treatment [125]. Thus, gaining insight into the cellular and molecular mechanisms involved in AVM formation will facilitate the development of targeted therapeutic strategies.

The present study focused on identifying the cellular and molecular mechanisms regulated by FSS and canonical BMP9 signaling crosstalk, their requirement in promoting and maintaining vascular quiescence, and how failure of this crosstalk results in AVMs.

The first part of my thesis identified Klf4 transcription factor and mechanosensor as a pivotal factor in AVM development. Klf4 is a transcription factor that modulates various EC functions, such as survival, migration, and proliferation [95]. Here, we (together with Kuheli Banerjee) identified that the physiological levels of Klf4 expression dictate vascular quiescence and protect the endothelium against AVMs. Klf4 abnormal expression can thus interfere with typical vascular homeostasis and foster aberrant angiogenesis. We found Klf4 expression to be upregulated specifically within the AVMs due to the increased sensitivity of AVM ECs to FSS, suggesting Smad4 signaling as yet another mechanism regulating FSS set point in ECs. Following this idea, in SMAD4-depleted cells, FSS mediates morphological responses already at very low levels, indicating a lowering in the FSS set point. This is insofar crucial for FSS-induced cell cycle arrest. Upon Smad4 depletion, the cell cycle inhibition occurs at a very low FSS magnitude, so there is an increase in the number of ECs within the AVMs. Interestingly, this upregulation of Klf4 is attributed to the disruption of SMAD4 signaling just in the context of FSS, indicating that Smad4 signaling alone does not regulate Klf4 expression levels. Still, somehow, Smad4 functions to restrict the Klf4 regulation upon FSS.

Under FSS, ECs encounter mechanical stimuli that can initiate modifications in gene expression, notably an increase in Klf4 levels [96]. In the absence of SMAD4, this regulatory response is intensified, culminating in the pathological manifestations associated with AVMs. These results underscore the role of Klf4 overexpression in response to modified mechanical stress and signaling disruptions as a crucial mechanism in AVM formation, suggesting that targeted inhibition of Klf4 may offer a promising therapeutic strategy for preventing or treating AVMs.

Previous studies reported that loss of BMP9-SMAD4 signaling results in an elevated PI3K/Akt pathway activity baseline by impacting the availability of PI3K at the cell membrane. The PI3K/Akt signaling cascade plays a crucial role in vascular remodeling, and it is a potential target for treatment in AVMs and other types of vascular malformations [42, 97]. Building on this discovery, the present study identified Klf4 upstream of PI3K/AKT signaling and TIE2. Furthermore, TIE2 is essential for Klf4-mediated AKT activation in response to FSS, highlighting this receptor's critical role in EC signaling. This upstream regulation of TIE2 subsequently amplifies PI3K/Akt, specifically within AVMs. This finding is further corroborated by the observed rescue of the inhibition of ANG2, a specific ligand for the TIE2 receptor [86].

The KLF4-TIE2-AKT signaling axis offers a significant mechanistic understanding of the pathogenesis of AVMs. In ECs lacking SMAD4, altered shear stress conditions result in the overexpression of KLF4, a pivotal factor driving aberrant vascular growth. TIE2 has been identified as a crucial mediator in this pathway, facilitating the activation of Akt upon FSS, which leads to EC dysfunction, further exacerbating the atypical vascular development associated with AVMs. These observations indicate that the inhibition of TIE2 signaling may effectively disrupt the KLF4-AKT pathway, thereby mitigating the detrimental endothelial responses contributing to AVM pathogenesis.

FSS sensing in EC cells takes place through the mechanosensitive junctional complex consisting of PECAM-1, VEGFR2/3, and VE-cadherin. FSS triggers force on PECAM-1, which leads to activation of VEGFRs, mediated by Src family members [101]. This leads to subsequent activation of the transcription factors KLF2 and KLF4, which regulate the expression of most flow-responsive genes [102]. It has been well-established that variations in flow magnitude and corresponding shear stress result in proportional adjustments in vessel diameter to restore the baseline shear stress level [103]. This indicates that ECs promote physiological vascular remodeling “to keep in check” FSS within a specific set point. Prolonged deviations from this optimal range consequently initiate readjustments in vessel diameter [104]. My study identified Smad4 signaling as an additional mechanism in regulating the FSS set point by restricting the Klf4 expression levels. Therefore, the absence of SMAD4 in EC results in a reduction in the FSS set point, increased levels of KLF4, and vascular remodeling. As depletion of Smad4 is permanent, the ECs undergo chronic remodeling without possibly restoring the physiological FSS and AVM formation. The mechanism of how FSS-induced KLF4 stabilizes blood vessels under normal physiological flow and how the same pathway’s overactivation promotes vascular remodeling remains unclear. Furthermore, another crucial question in the field is how Smad4 signaling restricts the FSS-mediated activation of Klf4 and the downstream signaling to maintain EC quiescence.

Thus, the second part of my thesis was focused on identifying the Klf4 upstream molecular mechanism. Using RNA-seq, I identified KIT RTK as crucial in FSS and BMP9 signaling crosstalk-mediated vascular quiescence. KIT gene and KIT protein levels are downregulated upon FSS irrespective of the FSS magnitude in an SMAD4-dependent manner. Interestingly,

additional mechanisms such as Kit phosphorylation could also influence Kit protein stability upon Smad4 LOF and FSS. In vivo, Kit was expressed little in the developing retinas in control conditions. Yet, Kit was highly expressed throughout the endothelium in retinas with Smad4 LOF in the ECs, thus validating the in vitro RNA-seq data.

Furthermore, I found that Kit acts upstream of Klf4, which regulates Akt expression levels through Erk5. This is among the mechanisms of how FSS mediates vascular quiescence and homeostasis. Upon Smad4 depletion, Kit occurs only upon Smad4 depletion.

Kit gene is a pivotal factor in the development of AVMs upon SMAD4 depletion. The research reveals that KIT expression is upregulated in SMAD4-deficient endothelial cells subjected to FSS conditions. This upregulation activates several downstream signaling cascades, namely AKT and ERK5.

RNA sequencing revealed that the absence of SMAD4 leads to a significant upregulation of RTKs, suggesting that RTK signaling may have a critical role in the hypersensitivity of SMAD4-deficient cells to FSS. This observation from the RNA sequencing data could be transferred to computational blood flow simulations within AVM, where the KIT expression is closely aligned with the simulated wall shear stress levels. Western blot analysis showed a similar trend, with KIT protein expression downregulated in response to high FSS. However, in SMAD4 knockdown cells, KIT protein was consistently upregulated under 12 dynes/cm^2 of FSS. This indicates that KIT expression is not solely regulated at the gene level but may also be modulated post-transcriptionally, as previously reported [90].

The investigation into the role of KIT in mechanotransduction has demonstrated that although KIT does not exhibit a significant function under normal physiological conditions, its importance becomes pronounced in pathological states, particularly in the absence of SMAD4. KIT knockdown resulted in a reduction of KLF4 expression in conditions of FSS only when SMAD4 was absent. This indicates that KIT mediates abnormal FSS-induced gene expression only in pathological conditions with SMAD4 LOF. These findings suggest that KIT may play a role in the pathophysiology of vascular diseases associated with abnormal shear stress, such as AVMs.

BMP9 signaling appears to play a crucial role in regulating KIT expression. BMP9 stimulation resulted in a notable downregulation of KIT, further enhanced by applying FSS. This observation indicates a synergistic interaction between BMP9 and shear stress in modulating KIT expression levels. Additionally, the finding that BMP9 downregulated KIT expression in both control cells and those with SMAD4 knockdown suggests that the regulation of KIT by BMP9 occurs through a mechanism that is only partially dependent on SMAD4. These findings add a potential new regulatory element on how BMP9/10 signaling and FSS maintain EC quiescence [98].

Notably, the activation of ERK5 signaling by KIT in response to shear stress occurs in a ligand-independent manner, indicating that FSS alone induces KIT activation without its canonical ligand SCF. In contrast, PI3k/Akt activation by KIT seems to rely solely on ligand binding, as

reported earlier[99]. Furthermore, this study confirms previous findings that ERK5 is responsible for mediating KLF4 expression [100, 101].

Furthermore, the study establishes that inhibiting KIT can mitigate AVM formation in Smad4-deficient murine models, thereby reinforcing the essential role of Kit in the pathogenesis of AVMs. Masitinib, which acts as a KIT inhibitor, has been shown to significantly diminish AVM development, suggesting that targeting KIT represents a promising therapeutic strategy. These findings underscore the therapeutic potential of Kit inhibition for addressing vascular anomalies such as AVMs.

VEGFRs and TIE receptors, the main RTKs on ECs play a crucial role in angiogenesis, endothelial cell proliferation, migration, and survival [72]. This study now identified KIT as a novel regulator of ECs quiescence. Under pathological conditions, KIT can further enhance PI3K/Akt signaling in a ligand-dependent manner while also inducing increased levels of KLF4 in the absence of the ligand. The activation of KIT upon ligand binding most likely induces dimerization and subsequent signaling [102]. However, as I have shown, the activation of the ERK5-KLF4 axis does not rely on the ligand. Therefore, the exact mechanism of how KIT is activated under these conditions remains unclear. Possible explanations include its activation upon FSS, as it has been shown for VEGFR2/3 [71], or through G protein-coupled receptors, which also act as mechanosensors [103] and can activate other RTKs [66].

My study elucidates the pivotal involvement of KIT-ERK5 signaling in the pathogenesis of AVMs, particularly in the framework of SMAD4 LOF. Overexpression of KLF4 upon FSS, and dysregulated BMP9/10 signaling pathway emerges as a crucial factor in the development of AVMs. Furthermore, this study underscores the indispensable role of the KLF4-TIE2 signaling axis in the activation of Akt and highlights the significance of KIT, ERK5 and KLF4 in AVM formation (Figure 25).

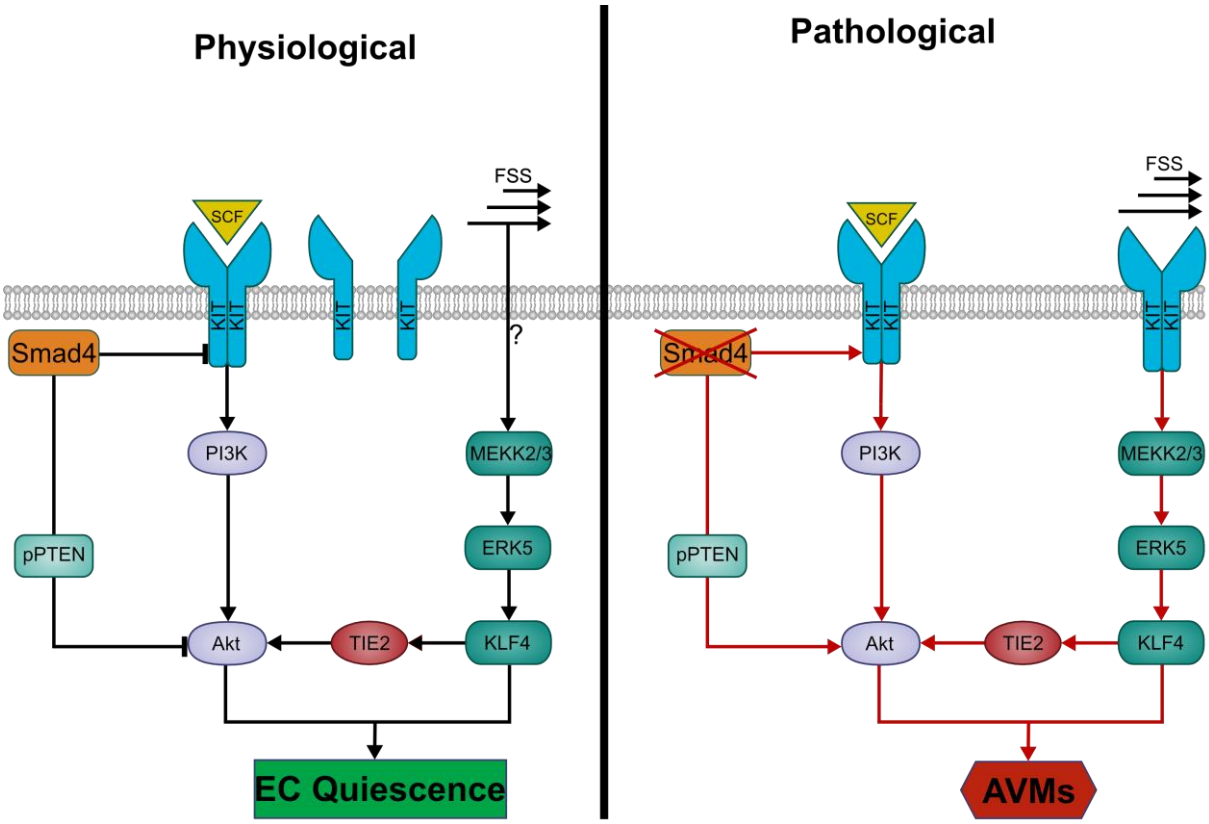

Figure 23: **Proposed molecular mechanism leading to AVM formation:** This study delineates the molecular processes responsible for the development of AVMs. The attached image illustrates the proposed signaling pathway based on the findings of this and previously published research. Smad4 is crucial in regulating FSS-induced ERK5 - KLF4 – TIE2 – PI3K/Akt signaling, facilitating EC quiescence. In the absence of Smad4, ECs become hypersensitive to FSS, triggering the activation of KIT signaling independent of its ligand SCF. This leads to the ERK5 - KLF4 – TIE2 – PI3K/Akt signaling cascade hyperactivation, ultimately resulting in AVM development.

5. Materials and Methods

5.1 Materials

5.1.1 Cell culture medium and reagents

Table 1: Cell culture medium and reagents

Components	Company	Catalog Number
HUVECs	Promocell	C-12203
Endothelial Cell Growth Medium MV 2	Promocell	C-22022
Penicillin/Streptomycin	Sigma-Aldrich	P4333-100ml
Fetal Bovine Serum (FCS)	Sigma-Aldrich	F-7524
Trypsin-EDTA	Sigma-Aldrich	T3924-500ml
Phosphate-buffered saline (PBS)	Sigma-Aldrich	D-5652
Opti-MEM™ Reduced Serum Medium	Thermo Fisher	31985070

5.1.2 Retina digestion buffers:

Table 2: Retina digestion buffers

Buffer	Amount	Contents
Fixation solution	4%	Paraformaldehyde (PFA)
Blocking buffer	1% 3%, 0.5% 0.01% 0.02%	FCS BSA Triton X-100 Sodium deoxycholate Sodium azide PBS
Wash buffer	1x	PBS

PBLEC buffer	1 mM 1 mM 1 mM 0.25%	$CaCl_2$ $MgCl_2$ $MnCl_2$ Triton X-100 PBS pH 7.4
Antibody dilution buffer	1X Blocking buffer	

5.1.3 Primary antibodies:

Table 3: Primary antibodies

Primary antibodies used for immunofluorescence			
Antibody	Company	Catalog Number	Dilution
Isolectin B4	Life Technologies	121412	10 µg/ml
KLF4	R&D systems	AF3158	1:200
SMA	Agilent	M0851	1:100
VE-cadherin	BD	555289	1:400
DAPI	Sigma-Aldrich	5087410001	1µg/ml
TIE2	R&D Systems	AF762	1:200
KIT	Agilent	A450229-2	1:200
Phospho-Erk5(Thr218/Tyr220)	Sigma-Aldrich	07-507	1:200
Primary antibodies used for immunoblots			
phospho-Akt (S473)	Cell Signaling	4060	1:1000
Akt	Cell Signaling	4685	1:1000
SMAD4	Cell Signaling	38454	1:1000
GAPDH	Cell Signaling	5174	1:10000
ERK5	Cell Signaling	3372	1:1000

TIE2	R&D Systems	AF313	1:1000
PECAM-1	Santa-Cruz	sc-376764	1:200
KIT	Cell Signaling	3074	1:1000
Phospho- Erk1/2 (Thr202/Tyr204)	Cell Signaling	4370	1:1000

5.1.4 Secondary antibodies

Table 4: Secondary antibodies

Antibody	Company	Catalog Number	Dilution
Alexa Fluor donkey anti-goat	Thermo Fisher	A-21432	1:250
Alexa Fluor donkey anti-rabbit	Thermo Fisher	R37118	1:250
Alexa Fluor donkey anti-rat	Thermo Fisher	A-21209	1:250
Alexa Fluor donkey anti-mouse	Thermo Fisher	**A-21202**	1:250
Horse Anti-Mouse Peroxidase	Vector Laboratories	VEC-PI-2000	1:5000
Goat Anti-Rabbit Peroxidase	Vector Laboratories	VEC-PI-1000	1:5000

5.1.5 Human small interfering RNA (siRNA)

Table 5: Human small interfering RNA (siRNA)

siRNA	Company	Catalog Number/Sequence
Control siRNAs	Dharmacon/Horizon	D-001810-01
Human *SMAD4* siRNA	Dharmacon/Horizon	L-003902-00
Human *KLF4* siRNA	Dharmacon/Horizon	M-005089-03
Human TEK siRNA	Dharmacon/Horizon	Q-003178-00

Human *ACVRL1* siRNA	Dharmacon/Horizon	L-005302-02
Human *SMAD1* siRNA	QIAGEN	SI00020027
Human *SMAD5* siRNA	QIAGEN	SI00082509
Human *KIT* siRNA	QIAGEN	SI00004837

5.1.6 RT-PCR Primers

Table 6:RT-PCR Primers

Gene name	Forward sequence	Reverse sequence
KIT	CGTTCTGCTCCTACTGCTTCG	CCCACGCGGACTATTAAGTCT
GAPDH	CTGGGCTACACTGAGCACC	AAGTGGTCGTTGAGGGCAATG
KLF4	CCCACATGAAGCGACTTCCC	CAGGTCCAGGAGATCGTTGAA
SMAD4	QT00013174, Qiagen	

5.1.7 Protein analysis buffers

Table 7: Protein analysis buffers

Buffer	Amount	Contents
Ponceau. S (100 ml)	0.2g 5 ml 95 ml	Ponceau acetic acid H_2O
TBS (10x)	100 mM 1.5 M	Tris pH: 7.4 NaCl
Western Blot buffer (10x) (1000 ml)	32.5 g 144 g	Tris Glycine

	1000 ml	H_2O
SDS-PAGE electrophoresis buffer (5X)	0.125M 1.25M 0.5%	Tris Glycine SDS H_2O
Tris buffer for stacking gel	1M	Tris pH 6.8
Tris buffer for resolving gel	1.5 M	Tris pH 8.8

5.1.8 Reagents

Table 8: Reagents

Reagent	Company	Catalog Number
Lipofectamine™ RNAiMAX	Thermo Fisher	13778150
Clarity Western ECL Substrate	Biorad	1705061
Roti-Mount FluorCare	Roth	HP19.1
PowerUp™ SYBR™ Green Master Mix	Thermo Fisher	A25777
CD31 Microbeads Mouse	Miltenyi Biotec	130-097-418
Tamoxifen	Sigma	T5648
Corn oil	Sigma	C8267
Laemmli buffer	Biorad	1610747
DNase I	Qiagen	79254

5.1.9 Kits

Table 9: Kits

Kits	Company	Catalog Number

RNeasy Plus Universal Mini Kit	Qiagen	73404
Quick-RNA-Miniprep kit	Zymo Research	R1055
Click-iT™ EdU Cell Proliferation Kit	Thermo Fisher	C10337
High-Capacity cDNA Reverse Transcription Kit	Thermo Fisher	4368813
PowerUp™ SYBR™ Green Master Mix	Thermo Fisher	A25778
Neural Tissue Dissociation Kit (P)	Miltenyi Biotec	130- 092-628

5.1.10 Chemicals

Table 10: Chemicals

Chemicals	Company	Catalog Number
APS	Merck	1.012.010.100
BSA	Sigma-Aldrich	A9647
DMSO	Sigma-Aldrich	D8418
PFA	Merck	1.040.031.000
Ponceau S	Sigma-Aldrich	P-3564
Precision Plus Protein	Biorad	1610395
Roti-Block	Roth	A151.1
TEMED	Roth	T7024
Tris	Serva	37181
Triton-X-100	Merck	1.080.031.000
Tween 20	Sigma-Aldrich	P-7949
Pictilisib	Selleck Chemicals	S1065
BIX02189	Selleck Chemicals	S1531
Imatinib Mesylate	MedChemExpress	HY-50946
Masitinib mesylate	MedChemExpress	HY-10209A

c-Kit-IN-5-1	MedChemExpress	HY-18302

5.1.11 Consumables

Table 11: Consumables

Material	Type	Company
Cell culture dishes	6 cm, 10 cm	Sarstedt
Cell culture flasks	T75 cm^2, T25 cm^2	Sarstedt
Cell culture multi-well plates	6-well, 12-well, 24-well	Sarstedt
Collecting tubes	50 mL, 15 mL	Sarstedt
Filter tips	1000 µL, 100 µL, 10µL	Greiner Bio One
MicroAmp® Fast Optical Reaction Plate	96-well, 0.2 mL	Applied Biosystems
MicroAmp® Optical Adhesive Film		Applied Biosystems
Microscope object slides	76×26 mm	R. Langenbrinck
Microscope square coverslips	24×24 mm, 24×60 mm	Carl Roth
PCR tubes	Multiply® µStrip Pro 8-strip	Sarstedt
Pipette tips	1000 µL, 100 µL, 10 µL	Sarstedt
Nitrocellulose membrane	2.5 µm	Whatman
Serological pipettes	5 mL, 10 mL, 25 mL	Sarstedt
Sterile syringes	Omnifix® solo 1 mL	B. Braun
µ-Slide VI 0.4 ibiTreat		Ibidi
Cell Strainer 70 µm Nylon	70 µm	Corning
MS columns		Miltenyi Biotec

5.1.12 Equipment

Table 12: Equipment

Equipment	Company
BioRad gel casting system	BioRad
BioRad gel running system	BioRad
BioRad Western Blotting equipment	BioRad
Cell culture hood	Thermo Fisher Scientific
Cell culture incubator	Thermo Fisher Scientific
Centrifuge	Thermo Fisher Scientific
Freezing box	Thermo Fisher Scientific
Pipettes	ErgoOne
Power supply	BioRad
Surgery and dissection tools	Fine Science Tools
Vortex	Neolab
Water bath	Julabo
Dissecting microscopes	Leica
Confocal	Zeiss LSM800
Pump system for shear stress	Ibidi
Orbital Shaker Rotamax120	Heidolph Instruments
Luminescent image analyser-Fusion FX	Vilber

5.1.13 Public Datasets

Table 13: Public Datasets

Dataset	Gene Expression Omnibus (GEO)	Reference
KLF4OE ChIP-Seq	GSE152900	[119]
Retinal scRNA-Seq	GSE175895	[121]

5.1.14 Software

Table 14: Software

Software	Company	Version
Graph Pad	Graph Pad	9.0
ZEN	Zeiss	3.10.103.00000
Fiji	ImageJ	2.16.0
Publisher 2	Affinity	2.5.7
Photo 2	Affinity	2.5.7
R	R Project	4.3.2
RStudio	Posit PBC	2024.09.1

5.1.15 R Packages

Table 15: R Packages

Software	Version
DESeq2	1.42.1
edgeR	4.0.16
ggplot2	3.5.1
dplyr	1.1.14
enrichplot	1.22.0
AnnotationDbi	1.64.1
RColorBrewer	1.1.3
org.Hs.eg.db	3.18.0
clusterProfiler	4.10.1
openxlsx	4.2.7.1
EnhancedVolcano	1.20.0
ggfortify	0.4.4

ggpubr	0.6.0
ggrepel	0.9.6
Seurat	5.1.0
Signac	1.14.0
patchwork	1.3.0.9000

5.2 Methods

5.2.1 Animal experiments:

Smad4 fl/fl (Smad4$^{tm2.1Cxd}$; Jackson Laboratory) and Klf4^{f}l/fl (B6.129S6-Klf4^{tm1Khk}; Mutant Mouse Resource Center) were mated with Tamoxifen (Tx)-inducible Cdh5-Cre^{ERT2} mice on a C57BL background to generate Smad4$^{i\Delta EC}$ and Klf4$^{i\Delta EC}$ mice. To create Smad4$^{i\Delta EC}$;Klf4$^{i\Delta EC}$ double knockout mice, Smad4$^{i\Delta EC}$ mice were further crossed with Klf4$^{i\Delta EC}$ mice. All animal handling procedures in this study received approval from the Animal Welfare Commission at the Regierungspräsidium Karlsruhe (Karlsruhe, Germany). To facilitate gene deletion, Tx (Sigma) was solubilized in corn oil (Sigma) at a concentration of 2 mg/ml and incubated overnight at 37°C. Intraperitoneal injections of 100 µg Tx were administered to pups at postnatal days P0-P2 in a volume of 50 µl. Mice were euthanized at P6. Cre-negative littermates received the same Tx treatment and were utilized as control subjects.

5.2.2Retina isolation and antibody staining:

The eyes of P6 pups were fixed in 4% paraformaldehyde (PFA) for 17 minutes at room temperature. Following fixation, the eyes were dissected under a microscope, and the retinas were carefully isolated. The isolated retinas underwent three washes with phosphate-buffered saline (PBS) and were subsequently incubated in a blocking buffer for 15 minutes at room temperature. The retinas were treated with specific primary antibodies, diluted in blocking buffer, and incubated overnight at 4°C. The following day, the retinas were washed and incubated with IB4 in conjunction with the appropriate secondary antibody in PBLEC buffer for 1 hour at room temperature, followed by a post-fixation step for 40 minutes at room temperature. Four radial incisions were made to flatten the retinal layers, allowing the structure to open into a four-leaf clover formation. The retinas were then mounted under a thin glass cover with RotiMount FluorCare (CarlRoth) as the mounting medium. Whole-mount retina images were captured using a Zeiss LSM800 confocal microscope equipped with an Airyscan Detector, and image processing was performed using the Zeiss ZEN software. A quantitative analysis of retinal vasculature was conducted using Fiji for further assessment.

5.2.3 Cell Culture:

Human umbilical cord vein endothelial cells (HUVECs) were purchased from Promocell and cultured in Endothelial Cell Growth Medium-MV2 (Promocell), supplemented with 1% penicillin/streptomycin (Sigma-Aldrich). The experiments were performed from passages 2 to 4. All cells were cultured under standard conditions at 37 °C in a 5% CO2 atmosphere.

5.2.4 Gene silencing with siRNA transfection:

siRNA transfection was conducted to achieve gene silencing in HUVECs. Specifically, 2 µL of siRNA was combined with 200 µL of serum-free medium (Opti-MEM, Life Technologies). Concurrently, 2 µL of Lipofectamine RNAiMAX Reagent (Life Technologies) was mixed with an additional 200 µL of Opti-MEM. This combined reagent mixture was incubated at room temperature for 20 minutes. Following incubation, the mixture was introduced to approximately 70% confluent HUVECs in 1 mL of culture medium to achieve a final siRNA concentration of 15pmol. After a culture period of 48 to 60 hours, the cells were prepared for subsequent experimental analysis.

5.2.5 Exposure of ECs to FSS:

Following transfection with siRNAs or overexpression constructs, a standardized number of HUVECs were seeded in 6-well plates, with 2 mL of growth medium allocated to each well. These plates were subsequently placed on an orbital shaker (Rotamax120, Heidolph Instruments) set to specific rotations per minute (rpm) to achieve shear stress levels of 1, 5, and 12 DYNES/cm². The rpm required for the desired shear stress level was calculated with the following formula[56]: $\tau max = a\sqrt{\eta\rho(2\pi f)^3}$, where a= orbital radius of rotation of the shaker in cm, η= viscosity of the medium, ρ= density of the culture medium and f= frequency of rotation (rotation/sec). Results from experiments carried out with the orbital shaker have been validated using an Ibidi pump system with the µ-Slide VI0.4 (Ibidi).

5.2.7 Isolation of Retina ECs:

Retinas from P6 pups were carefully dissected and dissociated using a modified version of the Neural Tissue Dissociation Kit (P). The tissue underwent a 5-minute digestion in buffer P, supplemented with DNase I at a concentration of 2000 U/ml. To stop digestion, fetal bovine serum (FBS) was added to achieve a final concentration of 10%. The resulting cell suspension was filtered through a 70µm cell strainer. Following centrifugation at 500g for 5 minutes, the cells were resuspended in PBS containing 2 mM EDTA and 0.5% BSA. For the enrichment of ECs, a selection was conducted using CD31 MicroBeads in accordance with the manufacturer's protocol.

5.2.7 Quantitative real-time polymerase chain reaction (RT-PCR):

Total cellular RNA was extracted utilizing the Quick RNA kit from Zymo Research, adhering strictly to the manufacturer's established protocol. The concentration of RNA was quantified using a NanoDrop ND-1000 spectrophotometer, with subsequent storage at -80 °C. An aliquot of RNA of 1 µg was used for reverse transcription, utilizing the High-Capacity cDNA Reverse

Transcription Kit (Thermo Fisher) as per the manufacturer's instructions. Normalization of the data was performed using GAPDH as internal control. All RT-PCR assays were conducted in duplicates, and the ΔCT method was applied to assess the variations in mRNA expression relative to the internal control.

5.2.8 Western Blot:

HUVECs were washed with PBS and subsequently lysed using Laemmli buffer (Bio-Rad). The resulting samples were subjected to separation via 10% sodium dodecyl sulfate-polyacrylamide gel electrophoresis (SDS-PAGE) and then transferred to 0.2 μm nitrocellulose membranes (GE Healthcare). Post-transfer, the membranes underwent three washes with TBST and were stained with 0.2% Ponceau S solution to verify the efficacy of protein transfer. After the staining confirmation, the membranes were rinsed with TBST to eliminate the Ponceau stain and subsequently blocked with Roti Block for 1 hour at room temperature. Following the blocking step, the membranes were incubated overnight at 4°C with the primary antibodies. On the subsequent day, the blots were washed three times for 10 minutes each with TBST and then incubated for 1 hour at room temperature with the respective secondary antibodies diluted in TBST. After incubation, the membranes were rewashed three times with TBST. For detection, Western blots were developed using the Clarity Western ECL Substrate (Bio-Rad) and analyzed on a Fusion FX luminescent image analyzer (Vilber). Band intensity was quantified utilizing ImageJ software.

5.2.9 RNA-seq Analysis:

The RNA-Seq reads were evaluated for quality using the MultiQC tool (version 1.13) and subsequently subjected to adapter trimming with Trimmomatic (version 0.39). Following this quality control process, the reads were aligned to the hg38 or mm10 reference genome utilizing STAR (version 2.7.10a) with specified parameters (-alignIntronMin 20 and -alignIntronMax 500,000). Tag directories were created using the makeTagDirectory function, and read counts were obtained through the analyzeRepeats.pl script (rna hg38 -strad both -count exons -noadj) from HOMER (version 4.7.2). Differential expression was quantified and normalized using DESeq2 (version 1.46.0). The Rpkm.default function from EdgeR was employed to calculate the average reads per million mapped (RPKM). Heatmaps were generated through heatmapper.ca, reflecting the row-based Z-scores derived from the RPKM values. Principal component analysis (PCA) plots were generated utilizing the prcomp function from the stats package within a customized R script (version 4.3.2). Additionally, volcano plots were created using the EnhancedVolcano R package (version 1.20.0). All datasets, including those available publicly, underwent normalization using consistent parameters.

5.2.10 Statistical analysis:

The data are presented as the mean ± standard error of the mean (S.E.M.). Each experiment was performed in triplicate and repeated independently at least three times. Statistical significance

between experimental groups was assessed using Student’s T-tests; for comparisons involving three or more groups, a one-way analysis of variance (ANOVA) was employed, followed by Tukey's post hoc test. A P value of less than 0.05 was considered statistically significant. All statistical analyses were conducted using GraphPad Prism 9.0.

6. Abbreviations

HHT	Hereditary Hemorrhagic Telangiectasia
AVM	Arteriovenous malformation
LOF	Loss-of-function
ACVRL1 or ALK1	Activin receptor-like kinase 1
SMAD4	SMAD family member 4
GDF2	Differentiation factors 2
BMP	Bone morphogenetic proteins
ECs	Endothelial cells
RTK	Receptor Tyrosine Kinase
CCM	Cerebral cavernous malformation
DLL4	Delta Like Canonical Notch Ligand 4
TEK	TEK Receptor Tyrosine Kinase
ENG	Endoglin
TIE1	Tyrosine Kinase With Immunoglobulin Like And EGF Like Domains 1
KDR	Kinase Insert Domain Receptor
FGFR1	Fibroblast Growth Factor Receptor 1
DDR1	Discoidin Domain Receptor Tyrosine Kinase
KIT	KIT Proto-Oncogene, Receptor Tyrosine Kinase
GAPDH	Glyceraldehyde-3-Phosphate Dehydrogenase
ERK	Extracellular Signal-Regulated Kinase
SCF	Stem cell factor
AKT	AKT Serine/Threonine Kinase
SMA	Smooth Muscle Actin

WSS	Wall shear stress
vSMCs	Vascular smooth muscle cells
bAVMs	Brain AVMs
VEGFA	vascular endothelial growth factor-A
Tx	Tamoxifen
VEGFR2	Vascular endothelial growth factor receptor 2
KLF4	Krüppel-like factor 4
FSS	Fluid shear stress
P-FSS	Physiological fluid shear stress
L-FSS	Low Fluid shear stress
H -FSS	High Fluid shear stress
FSS	Fluid shear stress
HUVECs	Human umbilical cord vein endothelial cells
PFA	Paraformaldehyde
WB	Western blotting
RT-PCR	Quantitative real-time polymerase chain reaction
CCM	Cerebral cavernous malformation
PECAM1	Platelet endothelial cell adhesion molecule 1
VE-cadherin	vascular endothelial cadherin
GPCR	G- protein-coupled receptor
NRP	Neuropilin
eNos	Endothelial nitric oxide synthase
Nrf2	nuclear factor-E2-related factor 2
MAPK	Mitogen-activated protein kinase
ERK	Extracellular Signal-Regulated Kinase
ANG	Angiopoietin

MEKK	Mitogen-activated Protein Kinase
SFK	Src family kinases
LDL	low-density lipoprotein
PDGFR	Platelet-Derived Growth Factor Receptor
FGFR	Fibroblast Growth Factor Receptor
PI3K	phosphoinositide 3-kinase
Akt	Akt kinase
mTOR	mammalian Target of Rapamycin
CK2	casein kinase 2
PAECs	pulmonary arterial endothelial cells
GO	Gene ontology
Dll4	Delta Like Canonical Notch Ligand 4
KDR	Kinase Insert Domain Receptor
RNA-seq	RNA sequencing
ChIP	chromatin immunoprecipitation

7. Units

°C	Degree Celsius
l	Liter
ml	Milliliter
µl	Microliter
g	Gram
mg	Milligram
µg	Microgram
M	Molar
mM	Millimolar
nmol	Nano mole
mol	Mole
µmol	Micro mole
cm	Centimeter
µm	Micrometer
cm^2	Centimeter squared
mm^2	Millimeter squared
h	Hour
min	Minute
U	Unit
V	Volt
rpm	revolutions per minute
DYNES/cm^2	Dynes per centimeter squared
Pa	Pascal

8. References

1. Shovlin CL, Guttmacher AE, Buscarini E, Faughnan ME, Hyland RH, Westermann CJ, et al. Diagnostic criteria for hereditary hemorrhagic telangiectasia (Rendu-Osler-Weber syndrome). Am J Med Genet. 2000;91(1):66-7.
2. Fuchizaki U, Miyamori H, Kitagawa S, Kaneko S, Kobayashi K. Hereditary hemorrhagic telangiectasia (Rendu-Osler-Weber disease). Lancet. 2003;362(9394):1490-4.
3. Kjeldsen AD, Vase P, Green A. Hereditary haemorrhagic telangiectasia: a population-based study of prevalence and mortality in Danish patients. J Intern Med. 1999;245(1):31-9.
4. Haitjema T, Westermann CJ, Overtoom TT, Timmer R, Disch F, Mauser H, et al. Hereditary hemorrhagic telangiectasia (Osler-Weber-Rendu disease): new insights in pathogenesis, complications, and treatment. Arch Intern Med. 1996;156(7):714-9.
5. Whitehead KJ, Smith MC, Li DY. Arteriovenous malformations and other vascular malformation syndromes. Cold Spring Harb Perspect Med. 2013;3(2):a006635.
6. McDonald J, Wooderchak-Donahue W, VanSant Webb C, Whitehead K, Stevenson DA, Bayrak-Toydemir P. Hereditary hemorrhagic telangiectasia: genetics and molecular diagnostics in a new era. Front Genet. 2015;6:1.
7. McDonald J, Bayrak-Toydemir P, Pyeritz RE. Hereditary hemorrhagic telangiectasia: an overview of diagnosis, management, and pathogenesis. Genet Med. 2011;13(7):607-16.
8. Hayama M, Maeda Y, Obata S, Tsuda T, Takeda K, Nishida T, et al. Understanding hereditary hemorrhagic telangiectasia: From genetic anomalies to systemic manifestations, quality of life, and epistaxis management-Exploring the otolaryngologist's integral role. Auris Nasus Larynx. 2024;51(2):305-12.
9. Cunha SI, Magnusson PU, Dejana E, Lampugnani MG. Deregulated TGF-beta/BMP Signaling in Vascular Malformations. Circ Res. 2017;121(8):981-99.
10. Snellings DA, Gallione CJ, Clark DS, Vozoris NT, Faughnan ME, Marchuk DA. Somatic Mutations in Vascular Malformations of Hereditary Hemorrhagic Telangiectasia Result in Bi-allelic Loss of ENG or ACVRL1. Am J Hum Genet. 2019;105(5):894-906.
11. Bernabeu C, Bayrak-Toydemir P, McDonald J, Letarte M. Potential Second-Hits in Hereditary Hemorrhagic Telangiectasia. J Clin Med. 2020;9(11).
12. McAllister KA, Grogg KM, Johnson DW, Gallione CJ, Baldwin MA, Jackson CE, et al. Endoglin, a TGF-beta binding protein of endothelial cells, is the gene for hereditary haemorrhagic telangiectasia type 1. Nat Genet. 1994;8(4):345-51.
13. Johnson DW, Berg JN, Baldwin MA, Gallione CJ, Marondel I, Yoon SJ, et al. Mutations in the activin receptor-like kinase 1 gene in hereditary haemorrhagic telangiectasia type 2. Nat Genet. 1996;13(2):189-95.
14. Howe JR, Roth S, Ringold JC, Summers RW, Jarvinen HJ, Sistonen P, et al. Mutations in the SMAD4/DPC4 gene in juvenile polyposis. Science. 1998;280(5366):1086-8.
15. Wooderchak-Donahue WL, McDonald J, O'Fallon B, Upton PD, Li W, Roman BL, et al. BMP9 mutations cause a vascular-anomaly syndrome with phenotypic overlap with hereditary hemorrhagic telangiectasia. Am J Hum Genet. 2013;93(3):530-7.
16. Li S, Wang SJ, Zhao YQ. Clinical features and treatment of hereditary hemorrhagic telangiectasia. Medicine (Baltimore). 2018;97(31):e11687.
17. Wu M, Chen G, Li YP. TGF-beta and BMP signaling in osteoblast, skeletal development, and bone formation, homeostasis and disease. Bone Res. 2016;4:16009.
18. Urist MR. A morphogenetic matrix for differentiation of bone tissue. Calcif Tissue Res. 1970:Suppl:98-101.

19. Wang RN, Green J, Wang Z, Deng Y, Qiao M, Peabody M, et al. Bone Morphogenetic Protein (BMP) signaling in development and human diseases. Genes Dis. 2014;1(1):87-105.
20. Morikawa M, Derynck R, Miyazono K. TGF-beta and the TGF-beta Family: Context-Dependent Roles in Cell and Tissue Physiology. Cold Spring Harb Perspect Biol. 2016;8(5).
21. Lowery JW, de Caestecker MP. BMP signaling in vascular development and disease. Cytokine Growth Factor Rev. 2010;21(4):287-98.
22. Li C, Guo B, Bernabeu C, Kumar S. Angiogenesis in breast cancer: the role of transforming growth factor beta and CD105. Microsc Res Tech. 2001;52(4):437-49.
23. Derynck R, Zhang YE. Smad-dependent and Smad-independent pathways in TGF-beta family signalling. Nature. 2003;425(6958):577-84.
24. Song JJ, Celeste AJ, Kong FM, Jirtle RL, Rosen V, Thies RS. Bone morphogenetic protein-9 binds to liver cells and stimulates proliferation. Endocrinology. 1995;136(10):4293-7.
25. Neuhaus H, Rosen V, Thies RS. Heart specific expression of mouse BMP-10 a novel member of the TGF-beta superfamily. Mech Dev. 1999;80(2):181-4.
26. David L, Mallet C, Mazerbourg S, Feige JJ, Bailly S. Identification of BMP9 and BMP10 as functional activators of the orphan activin receptor-like kinase 1 (ALK1) in endothelial cells. Blood. 2007;109(5):1953-61.
27. David L, Mallet C, Keramidas M, Lamande N, Gasc JM, Dupuis-Girod S, et al. Bone morphogenetic protein-9 is a circulating vascular quiescence factor. Circ Res. 2008;102(8):914-22.
28. Koch S, Tugues S, Li X, Gualandi L, Claesson-Welsh L. Signal transduction by vascular endothelial growth factor receptors. Biochem J. 2011;437(2):169-83.
29. Ola R, Kunzel SH, Zhang F, Genet G, Chakraborty R, Pibouin-Fragner L, et al. SMAD4 Prevents Flow Induced Arteriovenous Malformations by Inhibiting Casein Kinase 2. Circulation. 2018;138(21):2379-94.
30. Bourdeau A, Dumont DJ, Letarte M. A murine model of hereditary hemorrhagic telangiectasia. J Clin Invest. 1999;104(10):1343-51.
31. Arthur HM, Ure J, Smith AJ, Renforth G, Wilson DI, Torsney E, et al. Endoglin, an ancillary TGFbeta receptor, is required for extraembryonic angiogenesis and plays a key role in heart development. Dev Biol. 2000;217(1):42-53.
32. Oh SP, Seki T, Goss KA, Imamura T, Yi Y, Donahoe PK, et al. Activin receptor-like kinase 1 modulates transforming growth factor-beta 1 signaling in the regulation of angiogenesis. Proc Natl Acad Sci U S A. 2000;97(6):2626-31.
33. Urness LD, Sorensen LK, Li DY. Arteriovenous malformations in mice lacking activin receptor-like kinase-1. Nat Genet. 2000;26(3):328-31.
34. Torsney E, Charlton R, Diamond AG, Burn J, Soames JV, Arthur HM. Mouse model for hereditary hemorrhagic telangiectasia has a generalized vascular abnormality. Circulation. 2003;107(12):1653-7.
35. Hao Q, Su H, Marchuk DA, Rola R, Wang Y, Liu W, et al. Increased tissue perfusion promotes capillary dysplasia in the ALK1-deficient mouse brain following VEGF stimulation. Am J Physiol Heart Circ Physiol. 2008;295(6):H2250-6.
36. Choi H, Kim BG, Kim YH, Lee SJ, Lee YJ, Oh SP. BMP10 functions independently from BMP9 for the development of a proper arteriovenous network. Angiogenesis. 2023;26(1):167-86.
37. Choi EJ, Chen W, Jun K, Arthur HM, Young WL, Su H. Novel brain arteriovenous malformation mouse models for type 1 hereditary hemorrhagic telangiectasia. PLoS One. 2014;9(2):e88511.

38. Park SO, Wankhede M, Lee YJ, Choi EJ, Fliess N, Choe SW, et al. Real-time imaging of de novo arteriovenous malformation in a mouse model of hereditary hemorrhagic telangiectasia. J Clin Invest. 2009;119(11):3487-96.
39. Peacock HM, Tabibian A, Criem N, Caolo V, Hamard L, Deryckere A, et al. Impaired SMAD1/5 Mechanotransduction and Cx37 (Connexin37) Expression Enable Pathological Vessel Enlargement and Shunting. Arterioscler Thromb Vasc Biol. 2020;40(4):e87-e104.
40. Kim YH, Choe SW, Chae MY, Hong S, Oh SP. SMAD4 Deficiency Leads to Development of Arteriovenous Malformations in Neonatal and Adult Mice. J Am Heart Assoc. 2018;7(21):e009514.
41. Mahmoud M, Allinson KR, Zhai Z, Oakenfull R, Ghandi P, Adams RH, et al. Pathogenesis of arteriovenous malformations in the absence of endoglin. Circ Res. 2010;106(8):1425-33.
42. Hwan Kim Y, Vu PN, Choe SW, Jeon CJ, Arthur HM, Vary CPH, et al. Overexpression of Activin Receptor-Like Kinase 1 in Endothelial Cells Suppresses Development of Arteriovenous Malformations in Mouse Models of Hereditary Hemorrhagic Telangiectasia. Circ Res. 2020;127(9):1122-37.
43. Tual-Chalot S, Garcia-Collado M, Redgrave RE, Singh E, Davison B, Park C, et al. Loss of Endothelial Endoglin Promotes High-Output Heart Failure Through Peripheral Arteriovenous Shunting Driven by VEGF Signaling. Circ Res. 2020;126(2):243-57.
44. Jin Y, Muhl L, Burmakin M, Wang Y, Duchez AC, Betsholtz C, et al. Endoglin prevents vascular malformation by regulating flow-induced cell migration and specification through VEGFR2 signalling. Nat Cell Biol. 2017;19(6):639-52.
45. Tual-Chalot S, Mahmoud M, Allinson KR, Redgrave RE, Zhai Z, Oh SP, et al. Endothelial depletion of Acvrl1 in mice leads to arteriovenous malformations associated with reduced endoglin expression. PLoS One. 2014;9(6):e98646.
46. Garrido-Martin EM, Nguyen HL, Cunningham TA, Choe SW, Jiang Z, Arthur HM, et al. Common and distinctive pathogenetic features of arteriovenous malformations in hereditary hemorrhagic telangiectasia 1 and hereditary hemorrhagic telangiectasia 2 animal models--brief report. Arterioscler Thromb Vasc Biol. 2014;34(10):2232-6.
47. Ola R, Dubrac A, Han J, Zhang F, Fang JS, Larrivee B, et al. PI3 kinase inhibition improves vascular malformations in mouse models of hereditary haemorrhagic telangiectasia. Nat Commun. 2016;7:13650.
48. Crist AM, Lee AR, Patel NR, Westhoff DE, Meadows SM. Vascular deficiency of Smad4 causes arteriovenous malformations: a mouse model of Hereditary Hemorrhagic Telangiectasia. Angiogenesis. 2018;21(2):363-80.
49. Zhou HL, Jiang XZ, Ventikos Y. Role of blood flow in endothelial functionality: a review. Front Cell Dev Biol. 2023;11:1259280.
50. Tanaka K, Chen M, Prendergast A, Zhuang Z, Nasiri A, Joshi D, et al. Latrophilin-2 mediates fluid shear stress mechanotransduction at endothelial junctions. EMBO J. 2024;43(15):3175-91.
51. Sugden WW, Meissner R, Aegerter-Wilmsen T, Tsaryk R, Leonard EV, Bussmann J, et al. Endoglin controls blood vessel diameter through endothelial cell shape changes in response to haemodynamic cues. Nat Cell Biol. 2017;19(6):653-65.
52. Humphrey JD, Schwartz MA. Vascular Mechanobiology: Homeostasis, Adaptation, and Disease. Annu Rev Biomed Eng. 2021;23:1-27.
53. Baeyens N, Bandyopadhyay C, Coon BG, Yun S, Schwartz MA. Endothelial fluid shear stress sensing in vascular health and disease. J Clin Invest. 2016;126(3):821-8.

54. Li J, Zhao Y, Coleman P, Chen J, Ting KK, Choi JP, et al. Low fluid shear stress conditions contribute to activation of cerebral cavernous malformation signalling pathways. Biochim Biophys Acta Mol Basis Dis. 2019;1865(11):165519.
55. Davis MJ, Earley S, Li YS, Chien S. Vascular mechanotransduction. Physiol Rev. 2023;103(2):1247-421.
56. Dardik A, Chen L, Frattini J, Asada H, Aziz F, Kudo FA, et al. Differential effects of orbital and laminar shear stress on endothelial cells. J Vasc Surg. 2005;41(5):869-80.
57. Givens C, Tzima E. Endothelial Mechanosignaling: Does One Sensor Fit All? Antioxid Redox Signal. 2016;25(7):373-88.
58. Ranade SS, Qiu Z, Woo SH, Hur SS, Murthy SE, Cahalan SM, et al. Piezo1, a mechanically activated ion channel, is required for vascular development in mice. Proc Natl Acad Sci U S A. 2014;111(28):10347-52.
59. Albarran-Juarez J, Iring A, Wang S, Joseph S, Grimm M, Strilic B, et al. Piezo1 and G(q)/G(11) promote endothelial inflammation depending on flow pattern and integrin activation. J Exp Med. 2018;215(10):2655-72.
60. Mehta V, Pang KL, Rozbesky D, Nather K, Keen A, Lachowski D, et al. The guidance receptor plexin D1 is a mechanosensor in endothelial cells. Nature. 2020;578(7794):290-5.
61. Tzima E, Irani-Tehrani M, Kiosses WB, Dejana E, Schultz DA, Engelhardt B, et al. A mechanosensory complex that mediates the endothelial cell response to fluid shear stress. Nature. 2005;437(7057):426-31.
62. Li J, Hou B, Tumova S, Muraki K, Bruns A, Ludlow MJ, et al. Piezo1 integration of vascular architecture with physiological force. Nature. 2014;515(7526):279-82.
63. Menon NV, Su C, Pang KT, Phua ZJ, Tay HM, Dalan R, et al. Recapitulating atherogenic flow disturbances and vascular inflammation in a perfusable 3D stenosis model. Biofabrication. 2020;12(4):045009.
64. Gao JQ, Wang P, Yan JW, Ba LN, Shi PL, Wu HM, et al. Shear Stress Rescued the Neuronal Impairment Induced by Global Cerebral Ischemia Reperfusion via Activating PECAM-1-eNOS-NO Pathway. Front Cell Dev Biol. 2020;8:631286.
65. Ishii T, Warabi E, Mann GE. Mechanisms underlying unidirectional laminar shear stress-mediated Nrf2 activation in endothelial cells: Amplification of low shear stress signaling by primary cilia. Redox Biol. 2021;46:102103.
66. Doddaballapur A, Michalik KM, Manavski Y, Lucas T, Houtkooper RH, You X, et al. Laminar shear stress inhibits endothelial cell metabolism via KLF2-mediated repression of PFKFB3. Arterioscler Thromb Vasc Biol. 2015;35(1):137-45.
67. Ku DN, Giddens DP, Zarins CK, Glagov S. Pulsatile flow and atherosclerosis in the human carotid bifurcation. Positive correlation between plaque location and low oscillating shear stress. Arteriosclerosis. 1985;5(3):293-302.
68. Pfenniger A, Meens MJ, Pedrigi RM, Foglia B, Sutter E, Pelli G, et al. Shear stress-induced atherosclerotic plaque composition in ApoE(-/-) mice is modulated by connexin37. Atherosclerosis. 2015;243(1):1-10.
69. Wang Z, Wang F, Kong X, Gao X, Gu Y, Zhang J. Oscillatory Shear Stress Induces Oxidative Stress via TLR4 Activation in Endothelial Cells. Mediators Inflamm. 2019;2019:7162976.
70. Nayak L, Lin Z, Jain MK. "Go with the flow": how Kruppel-like factor 2 regulates the vasoprotective effects of shear stress. Antioxid Redox Signal. 2011;15(5):1449-61.
71. Paudel R, Fusi L, Schmidt M. The MEK5/ERK5 Pathway in Health and Disease. Int J Mol Sci. 2021;22(14).

72. Zhou Z, Rawnsley DR, Goddard LM, Pan W, Cao XJ, Jakus Z, et al. The cerebral cavernous malformation pathway controls cardiac development via regulation of endocardial MEKK3 signaling and KLF expression. Dev Cell. 2015;32(2):168-80.
73. Ma C, Geng B, Zhang X, Li R, Yang X, Xia Y. Fluid Shear Stress Suppresses Osteoclast Differentiation in RAW264.7 Cells through Extracellular Signal-Regulated Kinase 5 (ERK5) Signaling Pathway. Med Sci Monit. 2020;26:e918370.
74. Fang JS, Coon BG, Gillis N, Chen Z, Qiu J, Chittenden TW, et al. Shear-induced Notch-Cx37-p27 axis arrests endothelial cell cycle to enable arterial specification. Nat Commun. 2017;8(1):2149.
75. Franke RP, Grafe M, Schnittler H, Seiffge D, Mittermayer C, Drenckhahn D. Induction of human vascular endothelial stress fibres by fluid shear stress. Nature. 1984;307(5952):648-9.
76. Kwon HB, Wang S, Helker CS, Rasouli SJ, Maischein HM, Offermanns S, et al. In vivo modulation of endothelial polarization by Apelin receptor signalling. Nat Commun. 2016;7:11805.
77. Tzima E, Kiosses WB, del Pozo MA, Schwartz MA. Localized cdc42 activation, detected using a novel assay, mediates microtubule organizing center positioning in endothelial cells in response to fluid shear stress. J Biol Chem. 2003;278(33):31020-3.
78. Franco CA, Jones ML, Bernabeu MO, Geudens I, Mathivet T, Rosa A, et al. Dynamic endothelial cell rearrangements drive developmental vessel regression. PLoS Biol. 2015;13(4):e1002125.
79. Tuttle JL, Nachreiner RD, Bhuller AS, Condict KW, Connors BA, Herring BP, et al. Shear level influences resistance artery remodeling: wall dimensions, cell density, and eNOS expression. Am J Physiol Heart Circ Physiol. 2001;281(3):H1380-9.
80. Baeyens N, Nicoli S, Coon BG, Ross TD, Van den Dries K, Han J, et al. Vascular remodeling is governed by a VEGFR3-dependent fluid shear stress set point. Elife. 2015;4.
81. Robinson DR, Wu YM, Lin SF. The protein tyrosine kinase family of the human genome. Oncogene. 2000;19(49):5548-57.
82. Cadena DL, Gill GN. Receptor tyrosine kinases. FASEB J. 1992;6(6):2332-7.
83. Hubbard SR. Structural analysis of receptor tyrosine kinases. Prog Biophys Mol Biol. 1999;71(3-4):343-58.
84. Sudhesh Dev S, Zainal Abidin SA, Farghadani R, Othman I, Naidu R. Receptor Tyrosine Kinases and Their Signaling Pathways as Therapeutic Targets of Curcumin in Cancer. Front Pharmacol. 2021;12:772510.
85. Maruyama IN. Mechanisms of activation of receptor tyrosine kinases: monomers or dimers. Cells. 2014;3(2):304-30.
86. Yu X, Sharma KD, Takahashi T, Iwamoto R, Mekada E. Ligand-independent dimer formation of epidermal growth factor receptor (EGFR) is a step separable from ligand-induced EGFR signaling. Mol Biol Cell. 2002;13(7):2547-57.
87. He F, Chang C, Liu B, Li Z, Li H, Cai N, et al. Copper (II) Ions Activate Ligand-Independent Receptor Tyrosine Kinase (RTK) Signaling Pathway. Biomed Res Int. 2019;2019:4158415.
88. Herrlich A, Daub H, Knebel A, Herrlich P, Ullrich A, Schultz G, et al. Ligand-independent activation of platelet-derived growth factor receptor is a necessary intermediate in lysophosphatidic, acid-stimulated mitogenic activity in L cells. Proc Natl Acad Sci U S A. 1998;95(15):8985-90.
89. Guo G, Gong K, Wohlfeld B, Hatanpaa KJ, Zhao D, Habib AA. Ligand-Independent EGFR Signaling. Cancer Res. 2015;75(17):3436-41.

90. Sergina NV, Rausch M, Wang D, Blair J, Hann B, Shokat KM, et al. Escape from HER-family tyrosine kinase inhibitor therapy by the kinase-inactive HER3. Nature. 2007;445(7126):437-41.
91. Del Piccolo N, Sarabipour S, Hristova K. A New Method to Study Heterodimerization of Membrane Proteins and Its Application to Fibroblast Growth Factor Receptors. J Biol Chem. 2017;292(4):1288-301.
92. Usui R, Shibuya M, Ishibashi S, Maru Y. Ligand-independent activation of vascular endothelial growth factor receptor 1 by low-density lipoprotein. EMBO Rep. 2007;8(12):1155-61.
93. Jin ZG, Ueba H, Tanimoto T, Lungu AO, Frame MD, Berk BC. Ligand-independent activation of vascular endothelial growth factor receptor 2 by fluid shear stress regulates activation of endothelial nitric oxide synthase. Circ Res. 2003;93(4):354-63.
94. Wang X, Bove AM, Simone G, Ma B. Molecular Bases of VEGFR-2-Mediated Physiological Function and Pathological Role. Front Cell Dev Biol. 2020;8:599281.
95. Fong GH, Rossant J, Gertsenstein M, Breitman ML. Role of the Flt-1 receptor tyrosine kinase in regulating the assembly of vascular endothelium. Nature. 1995;376(6535):66-70.
96. Deng Y, Zhang X, Simons M. Molecular controls of lymphatic VEGFR3 signaling. Arterioscler Thromb Vasc Biol. 2015;35(2):421-9.
97. Plein A, Fantin A, Ruhrberg C. Neuropilin regulation of angiogenesis, arteriogenesis, and vascular permeability. Microcirculation. 2014;21(4):315-23.
98. Kim KL, Shin IS, Kim JM, Choi JH, Byun J, Jeon ES, et al. Interaction between Tie receptors modulates angiogenic activity of angiopoietin2 in endothelial progenitor cells. Cardiovasc Res. 2006;72(3):394-402.
99. Adams RH, Eichmann A. Axon guidance molecules in vascular patterning. Cold Spring Harb Perspect Biol. 2010;2(5):a001875.
100. Andrae J, Gallini R, Betsholtz C. Role of platelet-derived growth factors in physiology and medicine. Genes Dev. 2008;22(10):1276-312.
101. Oladipupo SS, Smith C, Santeford A, Park C, Sene A, Wiley LA, et al. Endothelial cell FGF signaling is required for injury response but not for vascular homeostasis. Proc Natl Acad Sci U S A. 2014;111(37):13379-84.
102. Ghigo A, Laffargue M, Li M, Hirsch E. PI3K and Calcium Signaling in Cardiovascular Disease. Circ Res. 2017;121(3):282-92.
103. Song M, Finley SD. Mechanistic insight into activation of MAPK signaling by pro-angiogenic factors. BMC Syst Biol. 2018;12(1):145.
104. Nishimoto S, Nishida E. MAPK signalling: ERK5 versus ERK1/2. EMBO Rep. 2006;7(8):782-6.
105. Bahar ME, Kim HJ, Kim DR. Targeting the RAS/RAF/MAPK pathway for cancer therapy: from mechanism to clinical studies. Signal Transduct Target Ther. 2023;8(1):455.
106. Zhang X, Simons M. Receptor tyrosine kinases endocytosis in endothelium: biology and signaling. Arterioscler Thromb Vasc Biol. 2014;34(9):1831-7.
107. Baeyens N, Larrivee B, Ola R, Hayward-Piatkowskyi B, Dubrac A, Huang B, et al. Defective fluid shear stress mechanotransduction mediates hereditary hemorrhagic telangiectasia. J Cell Biol. 2016;214(7):807-16.
108. Banerjee K, Lin Y, Gahn J, Cordero J, Gupta P, Mohamed I, et al. SMAD4 maintains the fluid shear stress set point to protect against arterial-venous malformations. J Clin Invest. 2023;133(18).
109. Abdelilah-Seyfried S, Ola R. Shear stress and pathophysiological PI3K involvement in vascular malformations. J Clin Invest. 2024;134(10).

110. Iriarte A, Figueras A, Cerda P, Mora JM, Jucgla A, Penin R, et al. PI3K (Phosphatidylinositol 3-Kinase) Activation and Endothelial Cell Proliferation in Patients with Hemorrhagic Hereditary Telangiectasia Type 1. Cells. 2019;8(9).
111. Wang C, Baker BM, Chen CS, Schwartz MA. Endothelial cell sensing of flow direction. Arterioscler Thromb Vasc Biol. 2013;33(9):2130-6.
112. Graupera M, Potente M. Regulation of angiogenesis by PI3K signaling networks. Exp Cell Res. 2013;319(9):1348-55.
113. Sako K, Fukuhara S, Minami T, Hamakubo T, Song H, Kodama T, et al. Angiopoietin-1 induces Kruppel-like factor 2 expression through a phosphoinositide 3-kinase/AKT-dependent activation of myocyte enhancer factor 2. J Biol Chem. 2009;284(9):5592-601.
114. Han C, Choe SW, Kim YH, Acharya AP, Keselowsky BG, Sorg BS, et al. VEGF neutralization can prevent and normalize arteriovenous malformations in an animal model for hereditary hemorrhagic telangiectasia 2. Angiogenesis. 2014;17(4):823-30.
115. Ruiz S, Zhao H, Chandakkar P, Papoin J, Choi H, Nomura-Kitabayashi A, et al. Correcting Smad1/5/8, mTOR, and VEGFR2 treats pathology in hereditary hemorrhagic telangiectasia models. J Clin Invest. 2020;130(2):942-57.
116. Crist AM, Zhou X, Garai J, Lee AR, Thoele J, Ullmer C, et al. Angiopoietin-2 Inhibition Rescues Arteriovenous Malformation in a Smad4 Hereditary Hemorrhagic Telangiectasia Mouse Model. Circulation. 2019;139(17):2049-63.
117. Tsaryk R, Yucel N, Leonard EV, Diaz N, Bondareva O, Odenthal-Schnittler M, et al. Shear stress switches the association of endothelial enhancers from ETV/ETS to KLF transcription factor binding sites. Sci Rep. 2022;12(1):4795.
118. Kato N, Prinz V, Dengler J, Vajkoczy P. Blood Flow Assessment of Arteriovenous Malformations Using Intraoperative Indocyanine Green Videoangiography. Stroke Res Treat. 2019;2019:7292304.
119. Moonen JR, Chappell J, Shi M, Shinohara T, Li D, Mumbach MR, et al. KLF4 recruits SWI/SNF to increase chromatin accessibility and reprogram the endothelial enhancer landscape under laminar shear stress. Nat Commun. 2022;13(1):4941.
120. Busada JT, Chappell VA, Niedenberger BA, Kaye EP, Keiper BD, Hogarth CA, et al. Retinoic acid regulates Kit translation during spermatogonial differentiation in the mouse. Dev Biol. 2015;397(1):140-9.
121. Zarkada G, Howard JP, Xiao X, Park H, Bizou M, Leclerc S, et al. Specialized endothelial tip cells guide neuroretina vascularization and blood-retina-barrier formation. Dev Cell. 2021;56(15):2237-51 e6.
122. Fodstad P, Dheyauldeen S, Rinde M, Bachmann-Harildstad G. Anti-VEGF with 3-week intervals is effective on anemia in a patient with severe hereditary hemorrhagic telangiectasia. Ann Hematol. 2011;90(5):611-2.
123. Lebrin F, Srun S, Raymond K, Martin S, van den Brink S, Freitas C, et al. Thalidomide stimulates vessel maturation and reduces epistaxis in individuals with hereditary hemorrhagic telangiectasia. Nat Med. 2010;16(4):420-8.
124. Parambil JG, Gossage JR, McCrae KR, Woodard TD, Menon KVN, Timmerman KL, et al. Pazopanib for severe bleeding and transfusion-dependent anemia in hereditary hemorrhagic telangiectasia. Angiogenesis. 2022;25(1):87-97.
125. Muster R, Ko N, Smith W, Su H, Dickey MA, Nelson J, et al. Proof-of-concept single-arm trial of bevacizumab therapy for brain arteriovenous malformation. BMJ Neurol Open. 2021;3(1):e000114.